FPSO Roll Motions

by
Spyros A. Kinnas, PhD, Ocean Engineering Group, Dept. of Civil Engineering, University of Texas at Austin

Final Project Report

Prepared for the Minerals Management Service
Under the MMS/OTRC Cooperative Research Agreement
1435-01-99-CA-31003
Task Order 18033
1435-01-04-CA35515
Task Order 35989
MMS Project Number 406

and

OTRC Industry Consortium

December 2005

OTRC Library Number: 12/05B157

"The views and conclusions contained in this document are those of the authors and should not be interpreted as representing the opinions or policies of the U.S. Government. Mention of trade names or commercial products does not constitute their endorsement by the U. S. Government".

For more information contact:

Offshore Technology Research Center
Texas A&M University
1200 Mariner Drive
College Station, Texas 77845-3400
(979) 845-6000

or

Offshore Technology Research Center
The University of Texas at Austin
1 University Station C3700
Austin, Texas 78712-0318
(512) 471-6989

A National Science Foundation Graduated Engineering Research Center

TABLE OF CONTENTS

Page

Table of Contents……..……..i

List of Figures……..……..ii

1. Introduction..... 1

2. Assessment of Effectiveness of Bilge Keels Using the Tools Developed Under this Contract 2

3. Phase I (2000-2002) 5

4. Phase II (2002-2003) 8

5. Phase III (2003-2005) 11

6. Benefits to Sponsors: 21

Publications and Theses Produced Under this MMS Contract: 21

Related Publications and References: 22

Appendix A: Formulation and Numerical Implementation of the Present Finite Volume Method 23

Appendix B: Formulation and Numerical Implementation of the Boundary Element Method 27

Appendix C: Definitions of Parameters and Hydrodynamic Coefficients 32

Appendix D: Roll Response Amplitude Operator 33

Unit Conversion Chart 41

LIST OF FIGURES

Figure **Page**

1.1 Computational domain and boundary conditions for a 2-D FPSO hull subject to roll motions..... 1
2.1 Generic FPSO Hull-form used for calculation of roll response..... 2
2.2 Comparison of roll RAO at Fn_b = 0.6 for different bilge keel lengths 3
2.3 Comparison of roll RAO at Fn_b = 0.8 for different bilge keel lengths 3
3.1 Original cell distribution for the solution of the Euler equations 6
3.2 Added mass (left) and damping coefficients (right) for a rectangular hull..... 7
4.1 Predicted force over one period (left) and grid detail (right), in the case of a vertical plate..... 9
4.2 Vorticity contours and streamlines predicted by (a) Euler solver and (b) Navier-Stokes solver at t=0.5×T. Instantaneous flow far upstream goes to the right..... 9
4.2 Vorticity contours and streamlines predicted by (a) Euler solver and (b) Navier-Stokes solver at t=0.5×T. Instantaneous flow far upstream goes to the right..... 9
4.3 Predicted and measured drag and inertia coefficient on a vertical plate subject to a horizontal sinusoidal gust. 10
4.4 Added mass and damping coefficient as predicted by an older version of the current method in the case of an FPSO hull with 4% bilge keels 10
5.1 Verification of the current method using the pressures predicted from the boundary element method in the case of a submerged hull without bilge keels (left), and the effect of Reynolds number on predicted pressures along hull in the case of a submerged hull with bilge keels. 11
5.2 Improved grid utilized by the present method; without bilge keels (left) and with bilge keels (right) 12
5.3 Definition of bilge keel length and three different orientations..... 12
5.4 Boundary conditions and computational domain for test problem of fixed hull with bilge keels subject to oscillating flow..... 13
5.5 Results for the test problem shown in the previous figure..... 13

5.6 The Moving Body/Linear Free-surface method (MBLF), and the moving body/non-linear boundary conditions (fully non-linear) method..... 14
5.7 The various contributions to the pressure distribution along the hull..... 14
5.8 The moment history and pressure distribution for an FPSO hull section with bilge keels subject to roll motion, at amplitude of 0.05 rad..... 15
5.9 The moment history and pressure distribution for an FPSO hull section with bilge keels subject to roll motion, at amplitude of 0.1 rad..... 15
5.10 Wave profiles predicted by the boundary element method using linear and non-linear free-surface boundary conditions for a 2D FPSO hull in roll with amplitude of 0.2 rad. 16
5.11 The latest predictions from our most recent method, compared with those measured and those predicted by other methods..... 17
5.12 Predicted vorticity contour plots of a FPSO hull with 4% bilge keels subject to roll motion at Fn=0.6, and at two different time steps 17
5.13 Pressure distributions on the hull at t/T=2.5 and t/T=2.75 (4% bilge keels and Fn=0.8). 18
5.14 Moment histories from the viscous solver and the potential solver (4% bilge keels and Fn=0.8)..... 18
5.15 The pressure distribution along the FPSO hull from the present viscous solver for varying grid sizes and time step sizes at t/T=0.5 with Fn=0.8..... 19
5.16 Effect of bilge keel length on predicted added mass (left) and damping (right) coefficients in roll for FPSO hull section. 19
5.17 Effect of bilge keel orientation on results; hydrodynamic coefficients in roll (left), and vorticity contours (right)..... 20
A.1 Grid indexing, (a) i,j indexing, (b) global indexing..... 25
A.2 Boundary conditions and flow domain. 25
B.1 Fluid domain and corresponding boundaries 27
D.1 Comparison of RAOs for Fn_b=0.6 and 0.8; Inviscid results with NO BILGE KEELS 36
D.2 Comparison of RAOs for Fn_b=0.6 and 0.8; Inviscid results with 4% BILGE KEELS 36

D.3 Comparison of RAOs for Fn_b=0.6 and 0.8; Viscous results with NO BILGE KEELS 37
D.4 Comparison of RAOs for Fn_b=0.6 and 0.8; Viscous results with 2% BILGE KEELS 37
D.5 Comparison of RAOs for Fn_b=0.6 and 0.8; Viscous results with 4% BILGE KEELS 38
D.6 Comparison of RAOs for Fn_b=0.6; Viscous and Inviscid results with NO BILGE KEELS 39
D.7 Comparison of RAOs for Fn_b=0.6; Viscous and Inviscid results with 4% BILGE KEELS 39
D.8 Comparison of RAOs for Fn_b=0.8; Viscous and Inviscid results with NO BILGE KEELS 40
D.9 Comparison of RAOs for Fn_b=0.8; Viscous and Inviscid results with 4% BILGE KEELS 40

1. Introduction

Motivation: FPSO (Floating Production systems for Storage and Off-loading) hulls have been reported to be subject to excessive roll motions (in some cases of 20 degrees amplitude), which may cause fatigue in mooring lines, disruption of operation, and discomfort to the crew. An economical solution to mitigate these roll motions is through the installation of bilge keels on these hulls.

Objective: Develop a robust, validated computational model to study the effects of bilge keel shapes (extent and orientation) on roll motions, and use this model to provide guidance on their design.

Approach and Results: We have embarked, since 2000, on an effort to develop a computational technique for the prediction of the hydrodynamic coefficients of 2-D hulls subject to roll. We have arranged the involved work in 3 phases:

- Phase I (2000-2002)
- Phase II (2002-2003)
- Phase III (2003-2005)

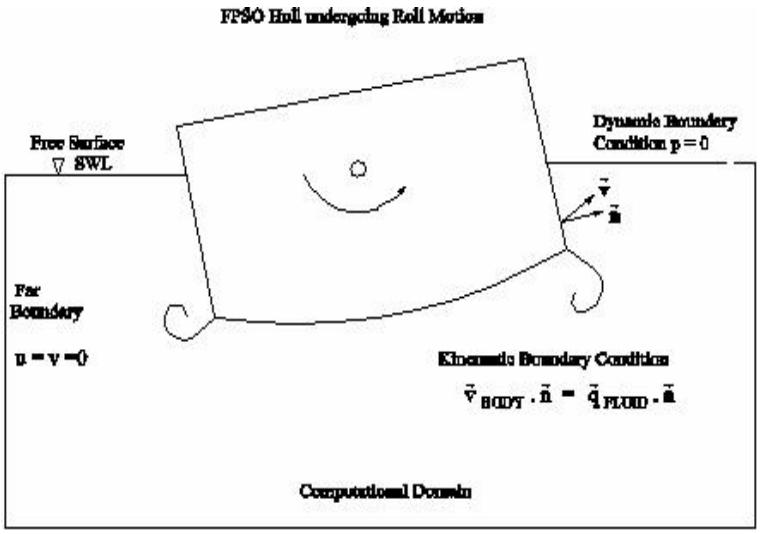

Figure 1.1: Computational domain and boundary conditions for a 2-D FPSO hull subject to roll motions.

The work performed under this project since 2000 will be summarized in the next pages. The reader can find additional information (including copies of theses, conference papers, presentations, and movies of results) on the FPSO web site at UT Austin:
http://cavity.ce.utexas.edu/kinnas/fpso/

2. Assessment of Effectiveness of Bilge Keels Using the Tools Developed Under this Contract

Before we describe in detail the approach for evaluating the hydrodynamic coefficients on an FPSO hull (without or with bilge keels), we present in this section how the outcome of our computational work has been used in order to assess the effectiveness of bilge keels in mitigating the response in roll for a realistic FPSO hull.

- Bilge keels provide an economical way to mitigate roll motions in FPSO hulls and the assessment of its effectiveness has been the focus of this project over the years. An ideal way to analyze the effectiveness of the bilge keels is through the study of the response of the hull to monochromatic beam seas by solving the appropriately constrained equations of motion (when analyzing roll, all the other degrees of freedom – surge, sway, heave, pitch and yaw, are assumed to be fixed).

- The response of the hull in an ambient wave field is commonly expressed in terms of a response amplitude operator (RAO) and is an important quantity in analyzing the effectiveness of bilge keels in FPSO hulls. In the case of roll-motion, the RAO gives a direct comparison between the amplitude of roll motion of the hull and the slope of the ambient wave field.

- Two important quantities that form an integral part in the calculation of the RAO are the added-mass and damping coefficients calculated by the different viscous and inviscid codes developed during the course of the project. These quantities are applied to a generic FPSO hull form as shown in Figure 2.1 in a strip-wise manner. The results of the analysis are presented in a concise form in Figures 2.2 and 2.3. A more detailed description of the solution of the equations of motion and calculation of the RAO is provided in Appendix D.

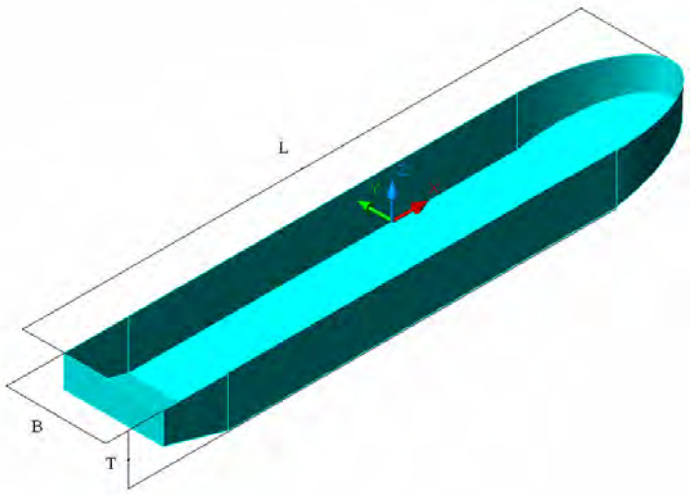

Figure 2.1 : Generic FPSO Hull-form used for calculation of roll response
(L = 270 m, B = 48 m, T = 24 m)

- In Figures 2.2 and 2.3, φ_a is the amplitude of roll motion, α_M is the slope of the incoming wave defined as H_M/L_M, Λ is the tuning factor (ratio of the wave encounter frequency to the natural roll frequency of the FPSO hull), Fn_b is the Froude number (defined in Appendix C). The ratio φ_a/α_M is the roll RAO.

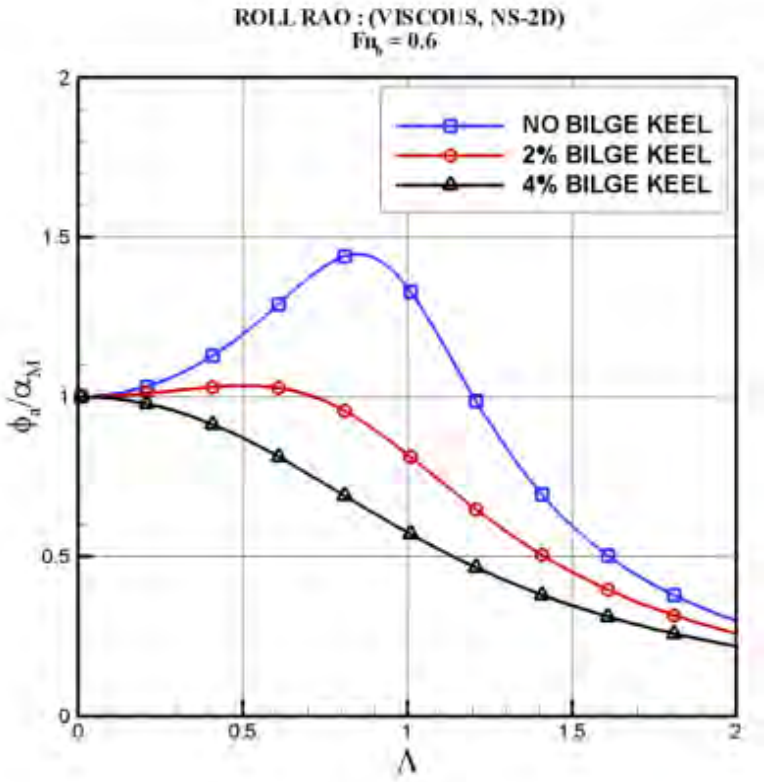

Figure 2.2 Comparison of roll RAO at Fn_b = 0.6 for different bilge keel lengths

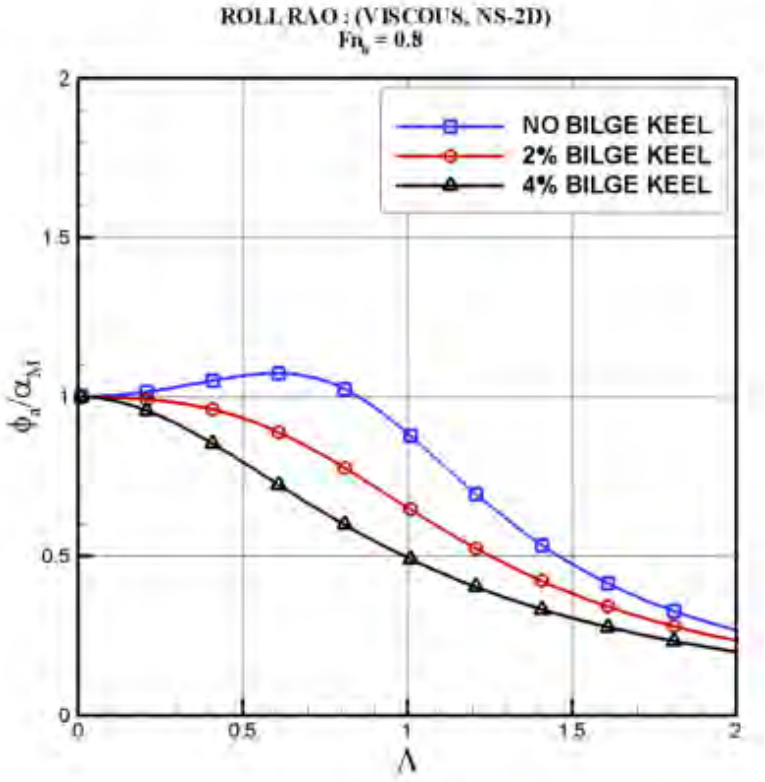

Figure 2.3 Comparison of roll RAO at Fn_b = 0.8 for different bilge keel lengths

Observations based on Roll RAO

- In the above figures, the response of the generic FPSO hull is calculated at two different frequencies expressed in terms of the Froude Number, $Fn_b = 0.6$ and 0.8. For a hull of B = 48 m, these Froude numbers correspond to wavelengths of 418 m (wave period = 16.38 s in deep water) and 235 m (wave period = 12.28 s in deep water) respectively.

- The effectiveness of the bilge keels is clearly illustrated in these Figures. In Figure 2.2, it can be observed that at $\Lambda = 0.8$, corresponding to a peak in the RAO for the no-bilge case), there is a *30%* reduction in the RAO with a bilge keel length of *2%B* and a *50%* reduction with a *4%B* bilge keel. A similar observation can be made in the case of the other frequency $Fn_b = 0.8$.

  In other words, for the FPSO hull we studied and the Froude no. of 0.6 a roll amplitude of 20 degrees in a bare hull, will be reduced to 14 degrees with a 2% bilge keel length, and to 10 degrees with 4% bilge keel length.

- A general overall and significant observation that can be made on the basis of this study is as follows:

  The effectiveness of the bilge keels in mitigating roll motions cannot be accurately predicted by the inviscid codes. This is due the fact that viscous effects in the vicinity of the bilge keels, which are not captured by the inviscid codes, play a major role in increasing the damping coefficient and hence decreasing the roll motion. Comparisons of viscid and inviscid solutions are presented in the figures in Appendix D.

3. Phase I (2000-2002)

In Phase I of this work, a previously developed method at UT Austin (Choi, PhD, 2000, Choi and Kinnas, 2000, 2003) for the prediction of 3-D unsteady flows around marine propellers was extended to predict the flow first around a 2-D vertical flat plate subject to a sinusoidal horizontal gust, and then the flow past an FPSO hull (without or with bilge keels) subject to heave or roll motions. The work was performed by an MS student with the Ocean Engineering Group in the Civil Engineering Department at UT, under the supervision of Prof. Kinnas. It should be noted that, due to the limited amount of funds in 2000-2001 (1/3 of the funds of those in subsequent years), only the second half of the related thesis was supported by OTRC/MMS, while the first half was supported by an independent international consortium on high-speed propulsors, led by the PI. The geometry of the problem in the case of an FPSO hull in roll is depicted in Fig. 1, while the most recent formulation of our solver for the unsteady Navier-Stokes equations (NS-2D) and the boundary conditions related to the FPSO roll problem, are summarized in Appendix A. The main characteristics of this method were (Kakar, UT MS, 2002):

- Node based finite volume method, 2^{nd} order accurate in space. The components of the velocity vectors and the pressure are defined at the nodes (corners) of the quadrilateral cells.

- Implicit Lax-Wendroff method, 2^{nd} order accurate in time

- Solved for the Euler equations (i.e. we ignored the effects of viscosity) and implemented 2^{nd} and/or 4^{th} order artificial dissipation terms to stabilize the solution (this also forced separation at the tip of the plate or at the tip of the bilge keel). In the case of the vertical flat plate we also solved for the Navier-Stokes equations in laminar flow.

- Solved for the velocity flow-field at each new time-step using the momentum equations, while the pressure was determined using the SIMPLE method in order to enforce the continuity equation at each time step.

In the case of an FPSO hull we:

- Implemented linearized kinematic and dynamic boundary conditions on the free surface.

- Applied the kinematic boundary condition on the mean body position (by imposing a flow velocity normal to the mean position of the body equal to the normal component of the rigid body velocity at the same location and time step).

- Applied appropriate conditions at the far boundaries, which were placed sufficiently far from the body to ensure that the flow around the body was not affected by reflections of the radiated waves at those boundaries. It should be mentioned that the current method can also be applied in the case of *shallow* depth water, even though most of the presented results are in the case of deep water.

The major findings of this phase were:

- The current method was able to predict separated flow downstream of sharp corners (e.g. the tip of a flat plate or that of a bilge keel).

- In the case of the vertical plate the predicted force over one period from the Euler or the Navier-Stokes method was found to be very close to each other. In other words solving for the Euler equations seemed to be sufficiently accurate. The most recent results from these studies will be presented under Phase II.

- In the case of 2-D FPSO hulls subject to heave motions the hydrodynamic coefficients were found to be well predicted over a wide range of Froude numbers by the current method, when compared to those using a boundary element approach or those measured by (Vugts 1968). The utilized grid in the case of an FPSO hull section with bilge keels is shown in Figure 3.1. The added mass and damping coefficients in heave vs. Froude number (also called reduced frequency) can be seen in Figure 3.2. Please note that the Euler equations solver and the boundary element method solver seem to predict the hydrodynamic coefficients in heave quite well over a wide range of Froude numbers.

- In the case of FPSO hulls subject to roll motions, however, the present method seemed to over predict the added mass and under-predict the damping coefficients, especially in the case of a bilge keel. The results from the current method seemed to be comparable to those produced by boundary element methods.

- The present method was able to predict the expected trend on the hydrodynamic coefficients with increasing bilge keel length.

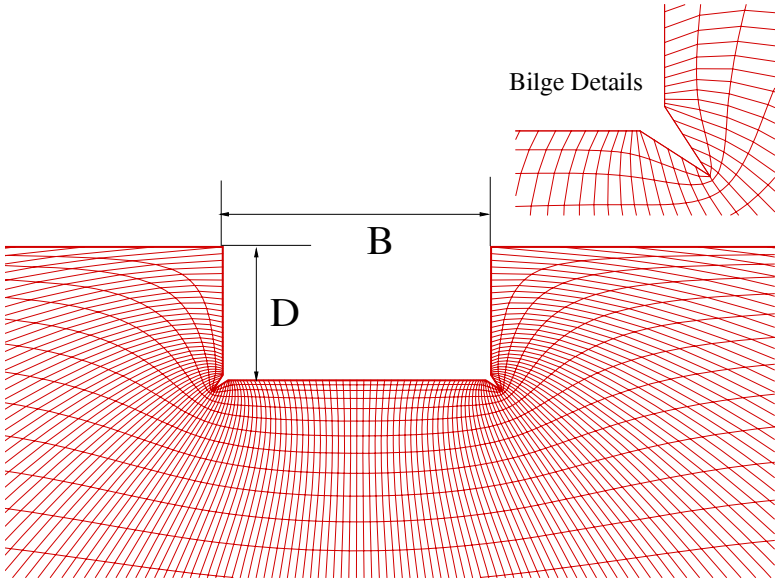

Figure 3.1: Original cell distribution for the solution of the Euler equations (Kakar 2002, Kinnas et al 2003). Note the high aspect ratio cells at the hull/free-surface intersection. A newer grid arrangement was introduced in Phase III which produced cells with aspects ratios closer to 1.

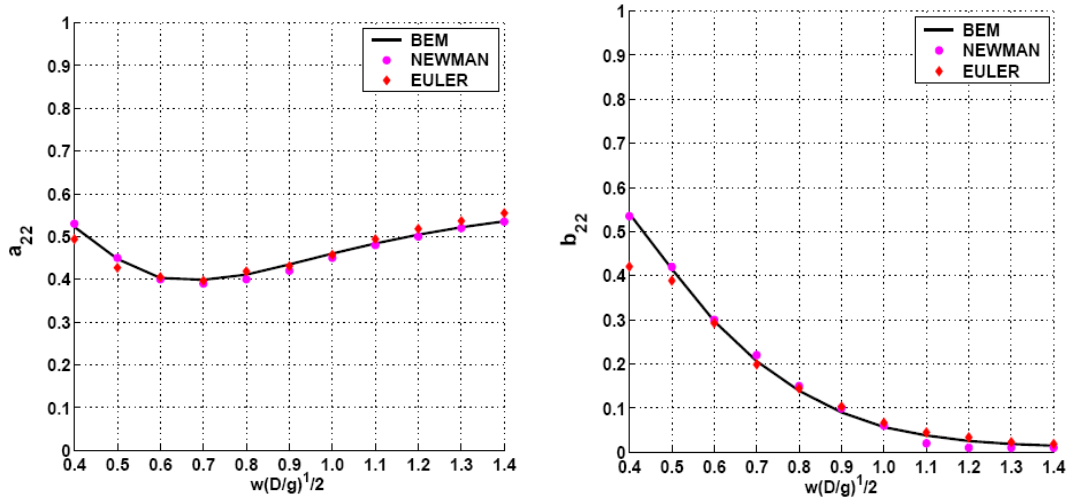

Figure 3.2: Added mass (left) and damping coefficients (right) for a rectangular hull (B/D=2) undergoing heave motion in deep-water, obtained by the present finite volume (Euler) method and the BEM solver, and compared to those obtained from the experiments of Vugts, 1968 (as presented in Newman, 1977).

4. Phase II (2002-2003)

In this Phase we validated the numerics of the current method, primarily in the case of the vertical flat plate. It should be noted that at this point of our research the results in the case of an FPSO hull did not seem to converge (i.e. the error in the solution seemed to grow with time) with significant changes in the grid resolution, and it was thus decided to investigate the behavior of the method in the case of the vertical plate first. The results of this effort were presented in the papers by Kinnas et al (12^{th} Offshore Symposium, 2003) and Kinnas et al (ISOPE, 2003). At this stage two new graduate students (Yu, PhD level, and Kacham, MS level) and a post-doctoral associate (Dr. H. Lee) performed this work under the supervision of Prof. Kinnas. The following changes were performed:

- The finite volume scheme was changed from a node based to a cell based. The components of the velocity vectors and the pressure were now defined at the centroids of the quadrilateral cells.

- Corrections were made in the treatment of the unsteady terms. In addition an implicit Crank-Nicolson scheme in time was implemented, and the pressure correction scheme was improved.

- The convective terms of the momentum equations were treated via an upwind 2^{nd} order differencing scheme

- In the case of the vertical plate convergence studies in terms of grid resolution and time step were performed, and our results were compared with those from commercial Navier-Stokes solver (Fluent) and experiments (Sarpkaya and O'Keefe 1995).

- The Navier-Stokes equations were implemented in the case of an FPSO hull

- The grid distribution was modified in order to improve the cell distribution at the free surface

- A boundary element method (with linearized free-surface conditions) was also developed in order to validate the current method in the case of inviscid flow and in the absence of bilge keels, but also in order to assess the effect of the separated flow (which the boundary element method cannot model) on the predictions in the case of bilge keels. The boundary element method (using linearized or non-linear boundary conditions) is summarized in Appendix B.

The outcome of our work on the oscillating flow around a plate is summarized in Figures 4.1, 4.2, and 4.3. Figure 4.1 shows that the results of our method compare well to those of a commercial code (Fluent). Figure 4.2 shows the predicted vorticity contours and streamlines using the Euler or the Navier-Stokes solver. Note that the differences between the two flow-fields are not significant, and this also results in pressures and forces on the plate, which do not vary significantly if the inviscid or viscous equations are solved. Figure 4.3 shows the comparisons of our predictions with the measurements of (Sarpkaya and O'Keefe1995). Finally, our methods were applied in the case of an FPSO hull subject to roll motion and the results from the boundary element method, the Euler and the Navier-Stokes solvers are given in Figure 4.4, together with those measured. The results are presented in terms of the added mass and damping coefficients, as defined in Appendix C. The lack of success of our method to predict hydrodynamic coefficients in roll which were closer to

measurements led us into Phase III, in which the numerics of our method were studied, and eventually drastically improved, in the case of an FPSO hull.

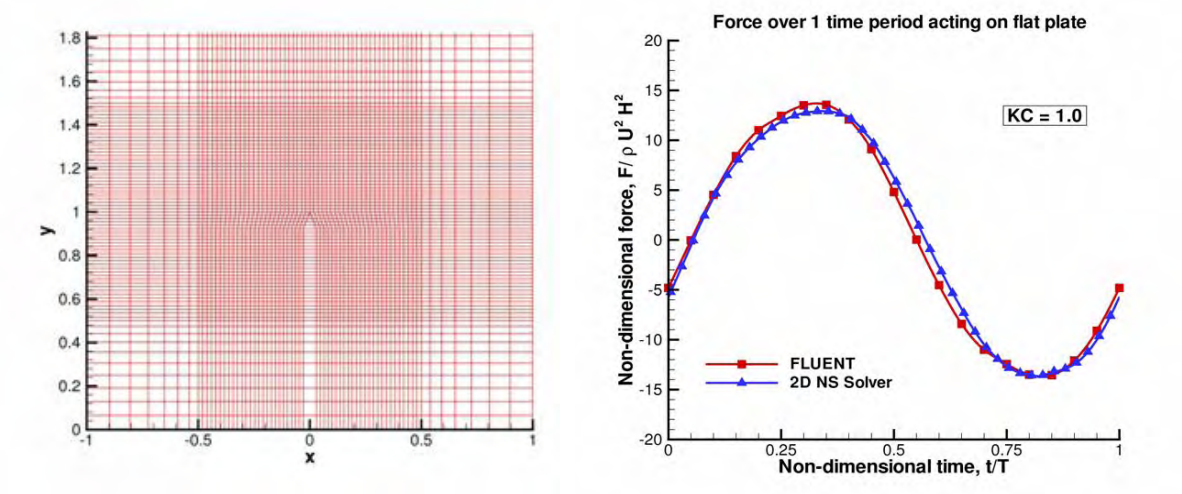

Figure 4.1: Predicted force over one period (left) and grid detail (right), in the case of a vertical plate.

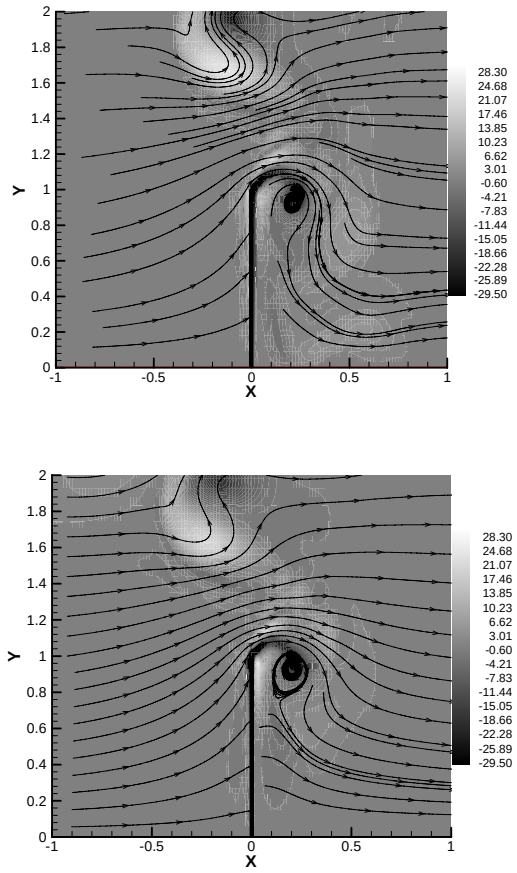

Figure 4.2. Vorticity contours and streamlines predicted by (a) Euler solver and (b) Navier-Stokes solver at t=0.5×T. Instantaneous flow far upstream goes to the right.

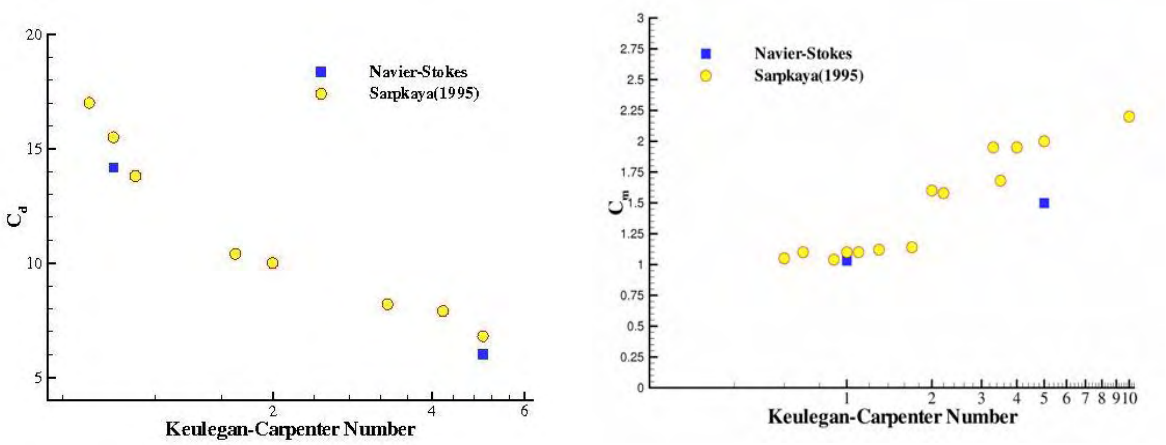

Figure 4.3: Predicted and measured drag and inertia coefficient on a vertical plate subject to a horizontal sinusoidal gust.

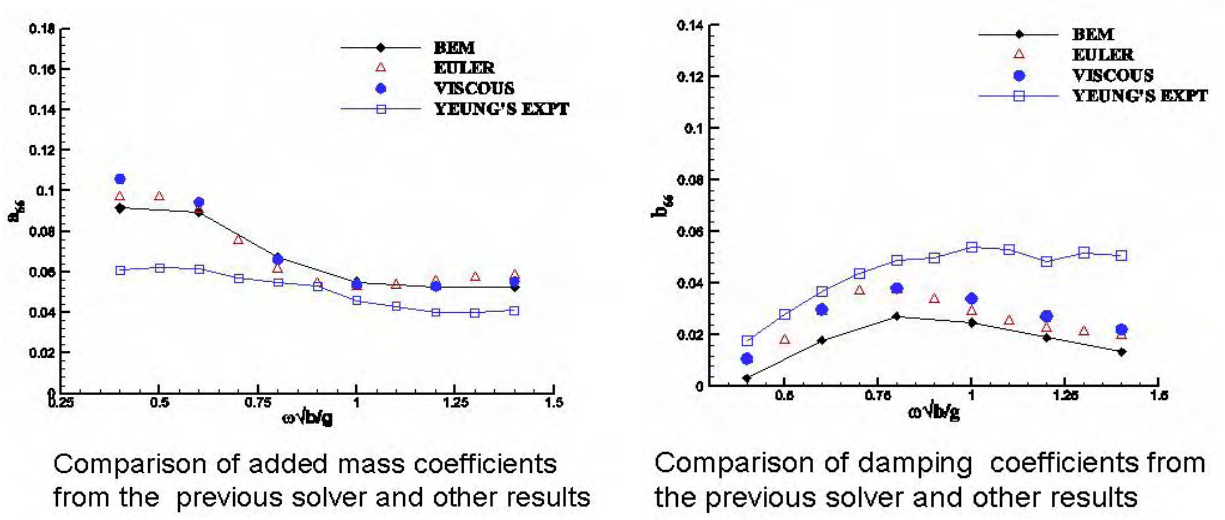

Comparison of added mass coefficients from the previous solver and other results

Comparison of damping coefficients from the previous solver and other results

Figure 4.4: Added mass and damping coefficient as predicted by an older version of the current method in the case of an FPSO hull with 4% bilge keels. IMPORTANT NOTE: The hull boundary conditions are applied on its mean location. It was found later in our research in Phase III that, as will also be presented in later figures, the boundary conditions had to be applied on the "exact" hull location in order for our predictions to come closer to the measurements.

5. Phase III (2003-2005)

At this stage an additional student (Vinayan, PhD level) was added to the research group. Some of the results of our research in Phase III have been reported in the MS Thesis of Kacham (2004) and more recent results will be reported in three papers by Kinnas et al which were presented at ISOPE 2005, OMAE 2005, and BeTeQ05. The following were accomplished in this phase, thus far:

- We studied the numerics of our method in the case of a fully submerged hull. In this way, the additional complexity of the free surface was factored out. In particular we compared the pressure distribution along the hull surface as predicted by the present method and a boundary element method (developed under Phase II). These comparisons led us to the introduction of the moving grid (see next item). One of these comparisons is shown in Figure 5.1 (left part). Please note that the very good agreement of the results from our method (in the absence of viscosity) with those of the potential method, as shown in Figure 5.1, was only achieved after the incorporation of the moving grid. It should also be noted that this case was used in order to find the proper grid resolution.

- We further improved the current method by including the effects of the moving grid in the Navier-Stokes equations, as described in Appendix A. The effects of the moving grid were also incorporated in the boundary element method. The effects of the Reynolds number on the pressure distribution are shown in Figure 5.1 (right part). Note that it is only for small Reynolds numbers (1000) that the predicted pressure distributions look different.

- We then applied the most recent method in the case of a hull with and without bilge keels and for various Froude numbers. The new grid (Kacham, 2004), as shown in Figure 5.2, avoids the high aspect ratio cells of the previous grid, as shown in Figure 3.1. The grid details and three different bilge keel orientations that we tested are shown in Figure 5.3. Using this new grid our method was run for a test problem in which an FPSO hull section with bilge keels is subject to a horizontal sinusoidal inflow with symmetry conditions applied on the free-surface (i.e. in the absence of waves), as depicted in Figure 5.4. The results (pressure distributions along the hull) from our method (NS-2D) and from Fluent are compared in Figure 5.5.

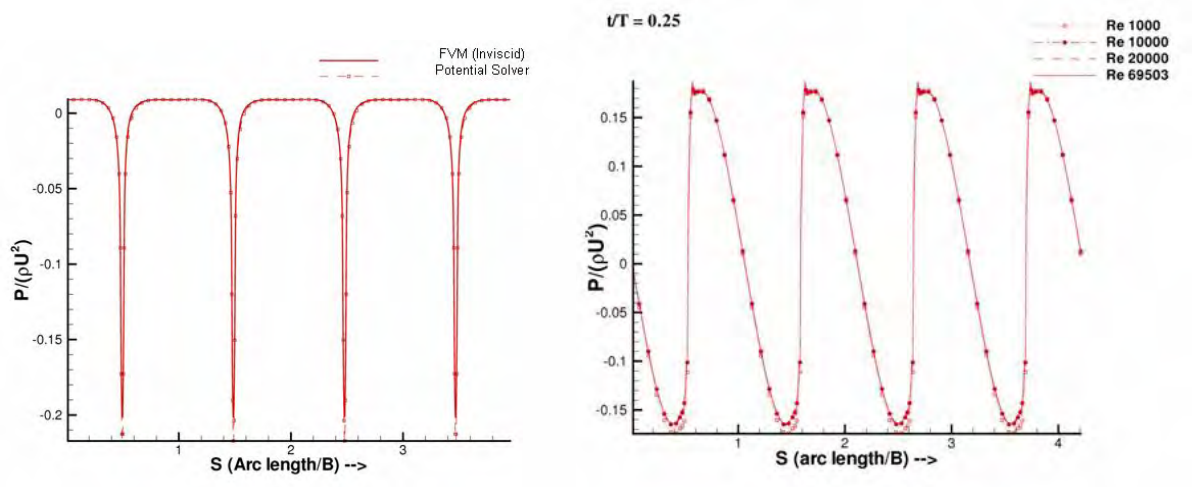

Figure 5.1: Verification of the current method using the pressures predicted from the boundary element method in the case of a submerged hull without bilge keels (left), and the effect of Reynolds number on predicted pressures along hull in the case of a submerged hull with bilge keels.

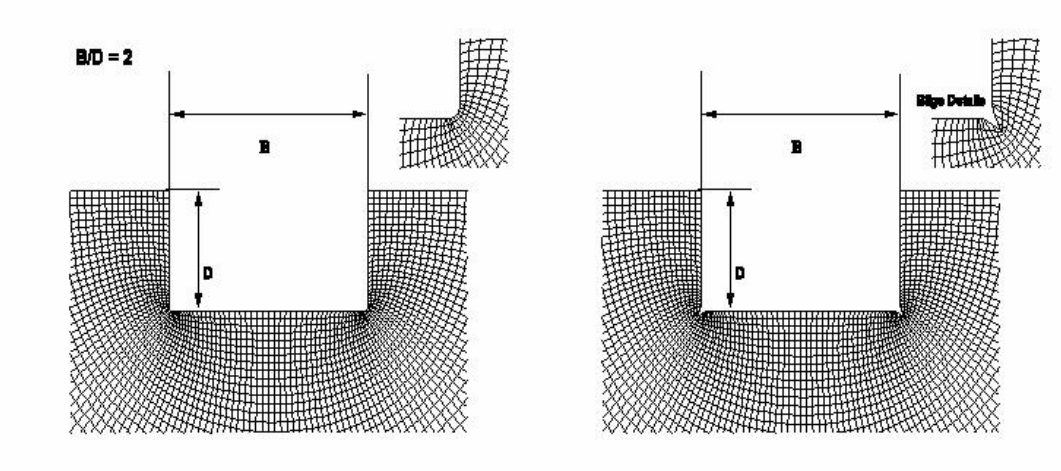

Figure 5.2: Improved grid utilized by the present method; without bilge keels (left) and with bilge keels (right) (Kacham, MS, UT 2004)

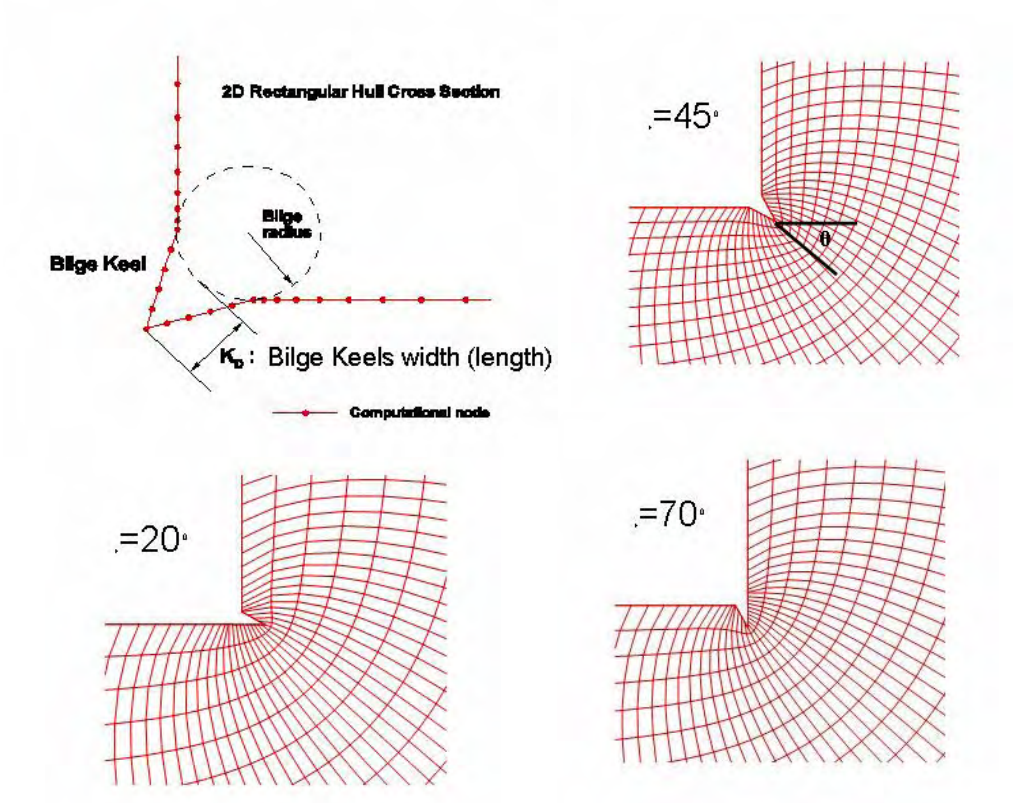

Figure 5.3: Definition of bilge keel length and three different orientations

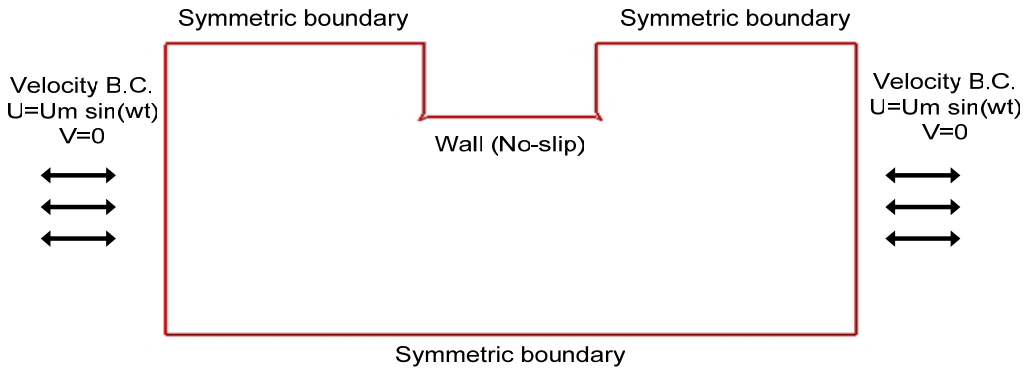

Figure 5.4: Boundary conditions and computational domain for test problem of fixed hull with bilge keels subject to oscillating flow.

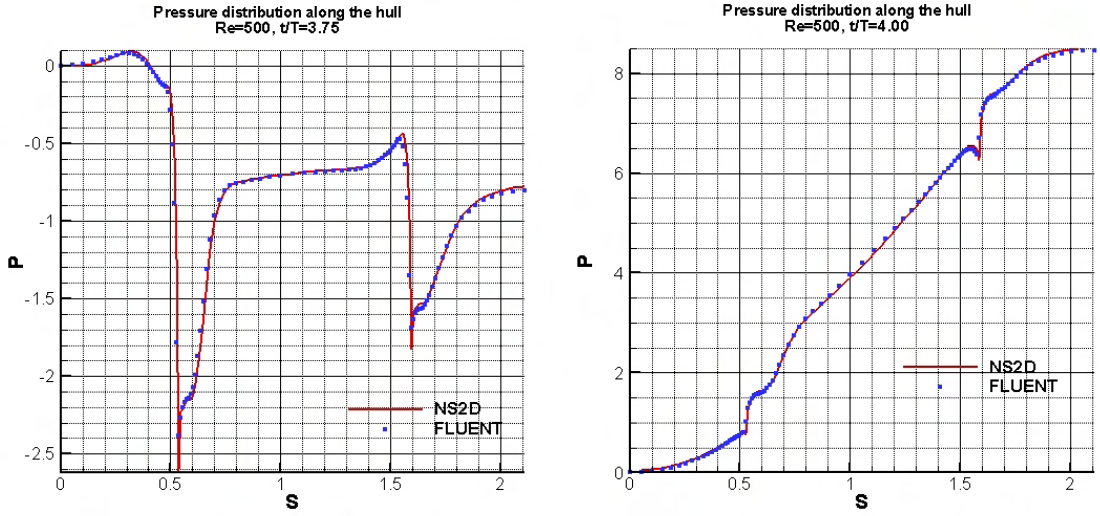

Figure 5.5: Results for the test problem shown in the previous figure. Comparison of the pressure distributions along the hull between NS2D and FLUENT at t/T=3.75 and 4.0 (Re=500).

- We finally modified our boundary element method (BEM) by incorporating the non-linear free-surface conditions. The formulation is summarized in Appendix B. This helped us quantify the effects of the currently used simplified linearized free surface conditions in our finite volume method. In particular, we studied the effects of the boundary conditions on the pressure distributions along the hull, by solving the following three problems via BEM: (a) purely linear, in which the body boundary conditions are applied in the mean position of the body and the linearized boundary conditions are applied on the free-surface; (b) MBLF, Moving Body with Linearized Free-surface conditions; and (c) fully non-linear in which non-linear conditions are applied on both the body and the free-surface. The MBLF and the fully non-linear approach are depicted on Figure 5.6. Results from the three approaches are shown in Figures 5.7-5.9. Please note that the pressures on the hull predicted from pure linear theory are quite different from those from non-linear theory (especially in the vicinity of the bilge keels), even at small roll amplitudes and even though

the roll moments (integrated pressures) are very close to each other. It is also VERY IMPORTANT to note that our MBLF approach predicts pressures along the hull which are quite close to those from non-linear theory. Having the correct pressure distribution along the hull is essential when applying our Navier-Stokes in the roll problem, and the application of the present MBLF approach has been found to improve our correlations with the measurements considerably (as will be shown next). Finally, Figure 5.10 shows comparisons of the predicted wave profiles using linear and non-linear free-surface conditions in the case of roll amplitude of 0.2 rad. Please note that the profiles are quite different close to the hull and this affects the values of the pressures and the extent of the wetted part of the hull (thus the value of the roll moment) significantly.

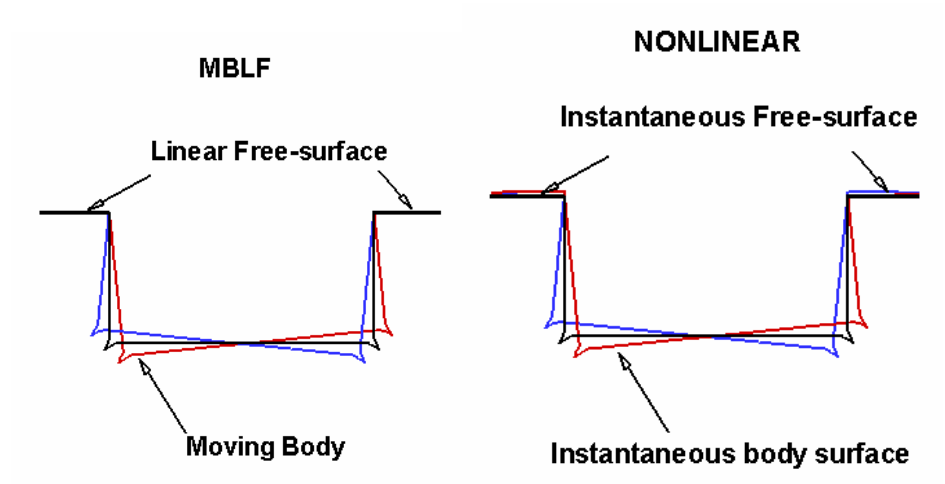

Figure 5.6: The Moving Body/Linear Free-surface method (MBLF), and the moving body/non-linear boundary conditions (fully non-linear) method

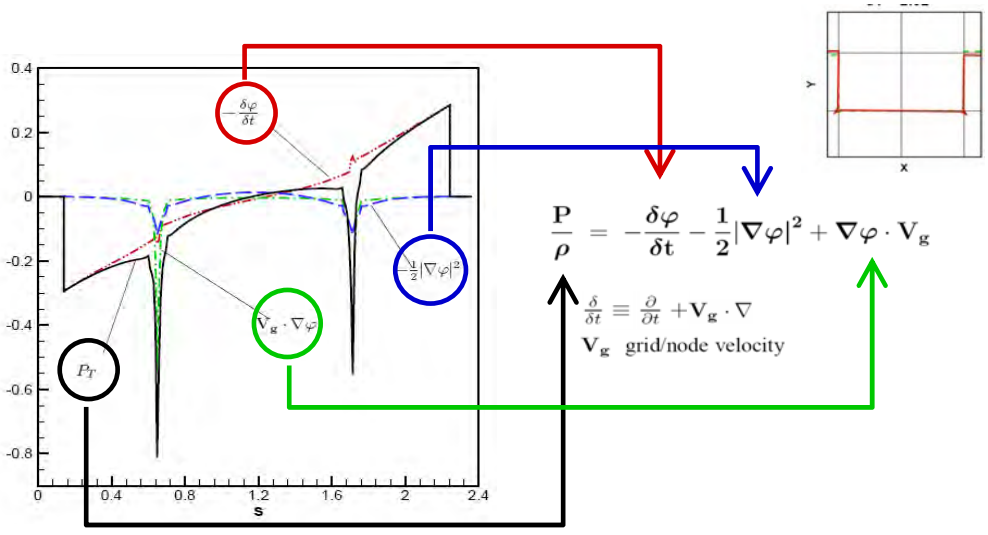

Figure 5.7: The various contributions to the pressure distribution along the hull. Note that the term in "red" corresponds to the pressure distribution in linear theory, and that its value is considerably different from the non-linear value of the pressure distribution (in "black"). The term in "blue" corresponds to the velocity terms of the Bernoulli equation, and the term in "green" corresponds to the terms due to the moving grid.

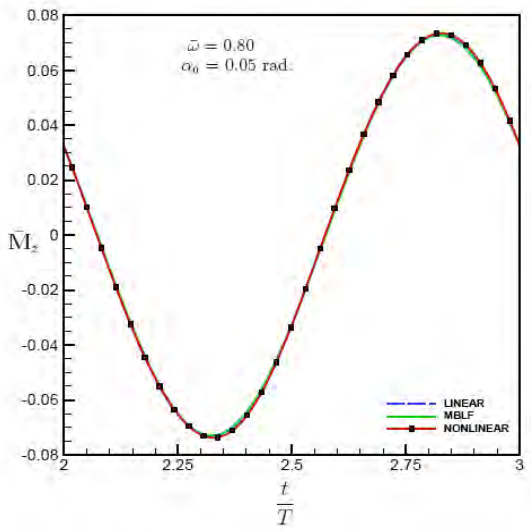

Roll Moment History, $\alpha_0 = 0.05, \bar{\omega} = 0.8$

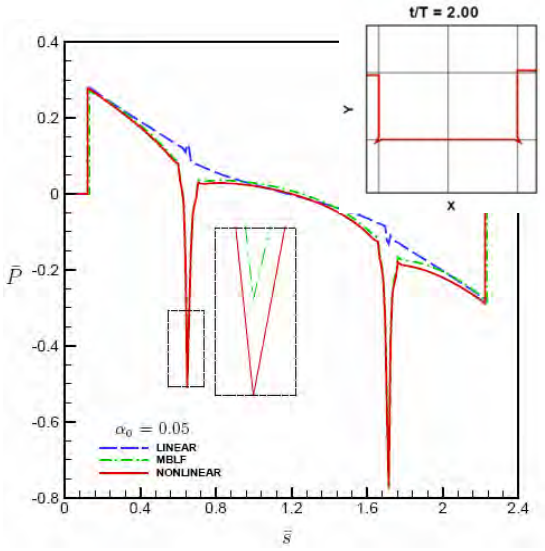

Pressure Distribution along Hull : $\bar{\omega}$=0.8, $\frac{t}{T}$=2.00, $\alpha_0 = 0.05$

Figure 5.8: The moment history and pressure distribution for an FPSO hull section with bilge keels subject to roll motion, at amplitude of 0.05 rad. Note the all theories predict practically the same moment, but that only MBLF produces pressures which are very close to those from fully non-linear theory.

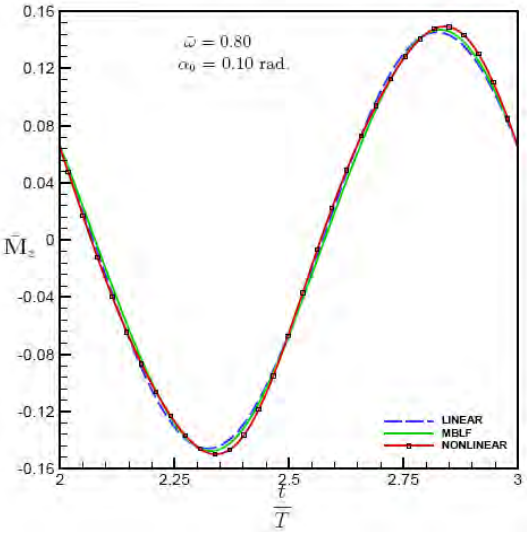

Roll Moment History, $\bar{\omega} = 0.80$, α_0=0.10

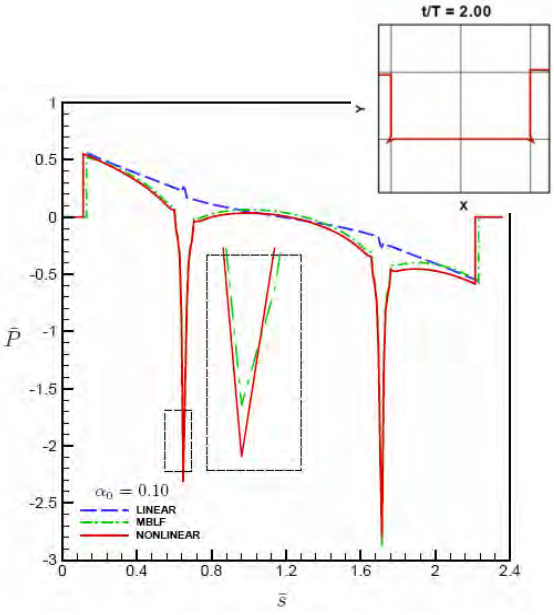

Pressure Distribution along Hull : $\bar{\omega}$=0.8, $\frac{t}{T}$=2.00, $\alpha_0 = 0.10$

Figure 5.9: The moment history and pressure distribution for an FPSO hull section with bilge keels subject to roll motion, at amplitude of 0.1 rad. Note all theories predict practically the same moment, but that only MBLF produces pressures which are very close to those from fully non-linear theory.

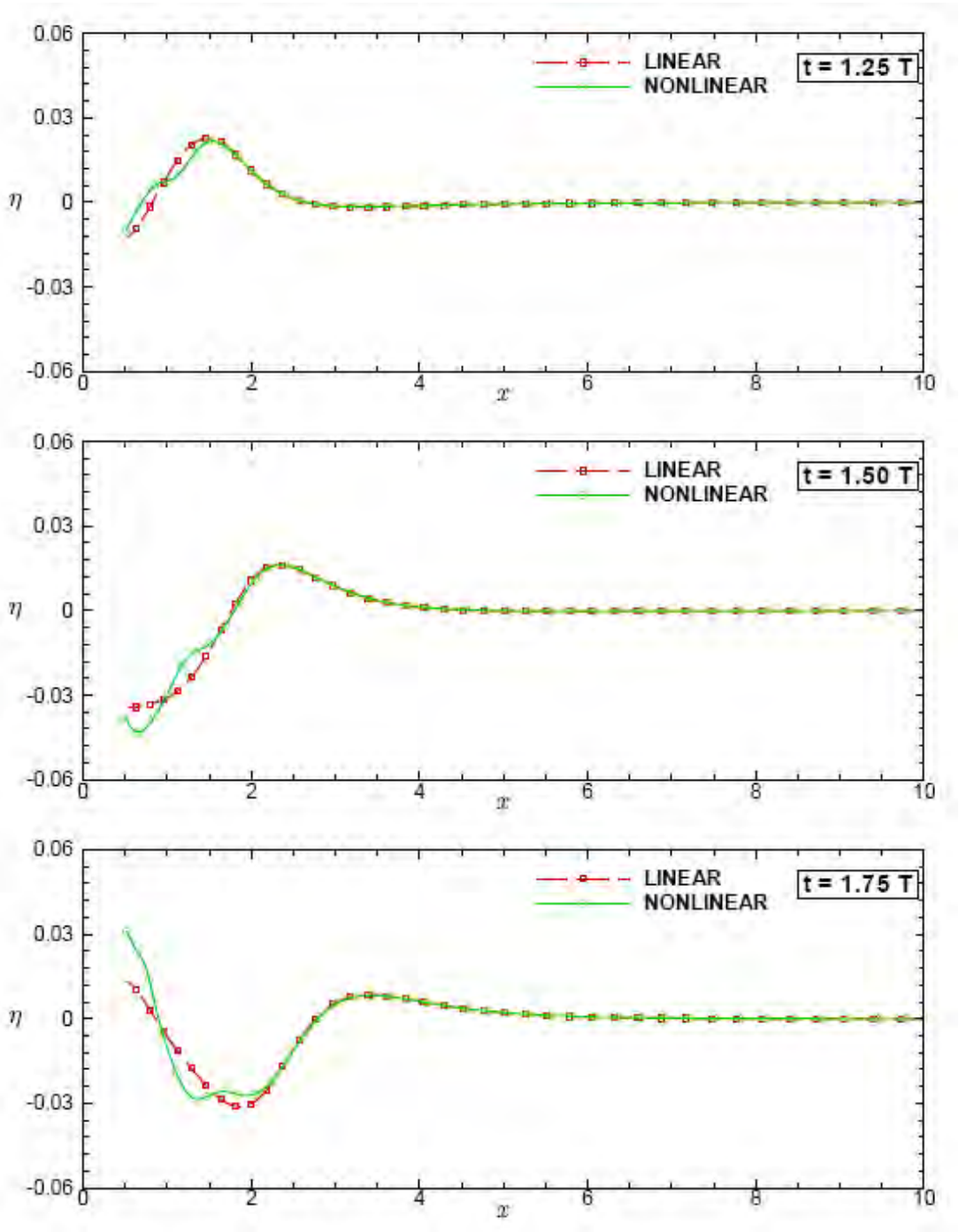

Figure 5.10: Wave profiles predicted by the boundary element method using linear and non-linear free-surface boundary conditions for a 2D FPSO hull in roll with amplitude of 0.2 rad.

- In the case of an FPSO hull in roll motion, the most recent results of our method are shown in Figure 5.11, where the added mass and damping coefficients are compared with measurements and other numerical results, (Yeung et al 2000). Figure 5.12 shows the predicted vorticity contours. Please note the significant improvement of our newest results, in comparison to the results of the older version of our method, as shown in Figure 4.4.

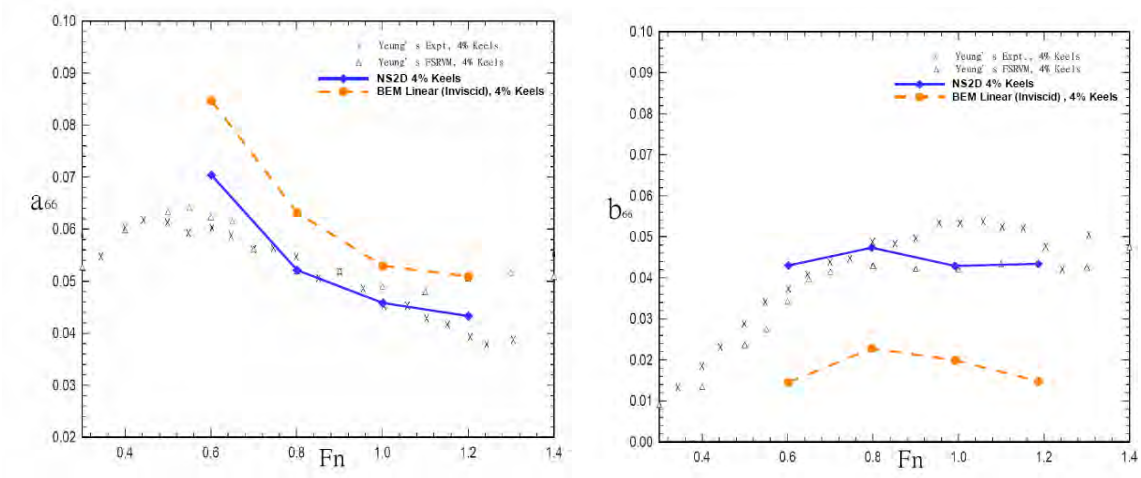

Figure 5.11: The latest predictions from our most recent method, compared with those measured and those predicted by other methods. Added mass (left) and damping coefficients (right)

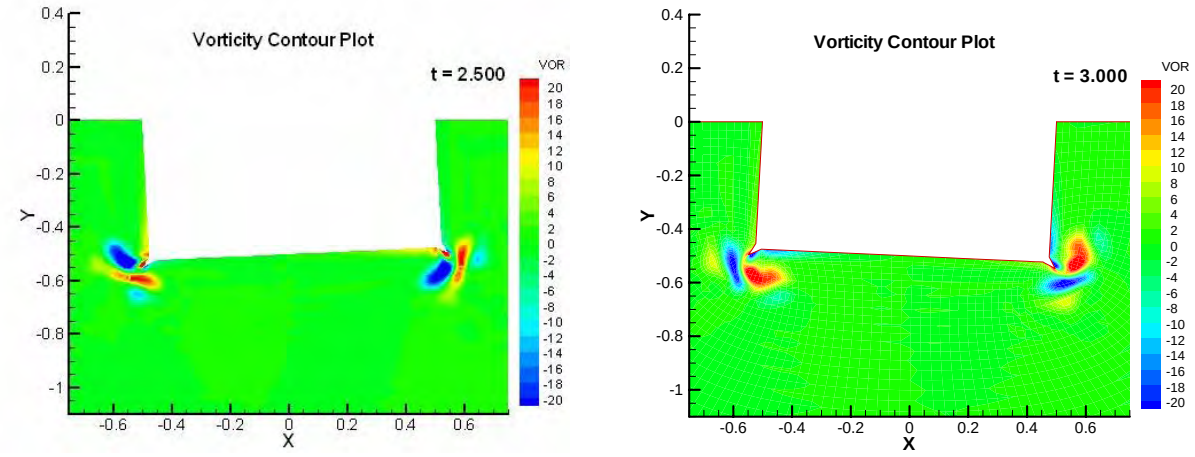

Figure 5.12: Predicted vorticity contour plots of a FPSO hull with 4% bilge keels subject to roll motion at Fn=0.6, and at two different time steps

- The pressure distributions from all inviscid and the viscous method are compared in Figures 5.13 and 5.14, in terms of pressure distributions and time history of roll moments. As expected the effects of viscosity are significant.

- Several grid dependence studies were performed, and a representative result from these studies is shown in Figure 5.15.

- The effect of bilge keel length on the results is shown in Figure 5.16. As expected both the added mass and the damping coefficients increase with increasing bilge keel length, even though the latter increases faster than the former.

- The effect of the bilge keel orientation was studied and results are shown in Figure 5.17. It should be noted that our method seems to predict the same effect of bilge keel orientation on the results as those measured in Na et al (2002) or predicted by Seah and Yeung (2003), despite the fact that our bilge keel geometry is not the same to that tested.

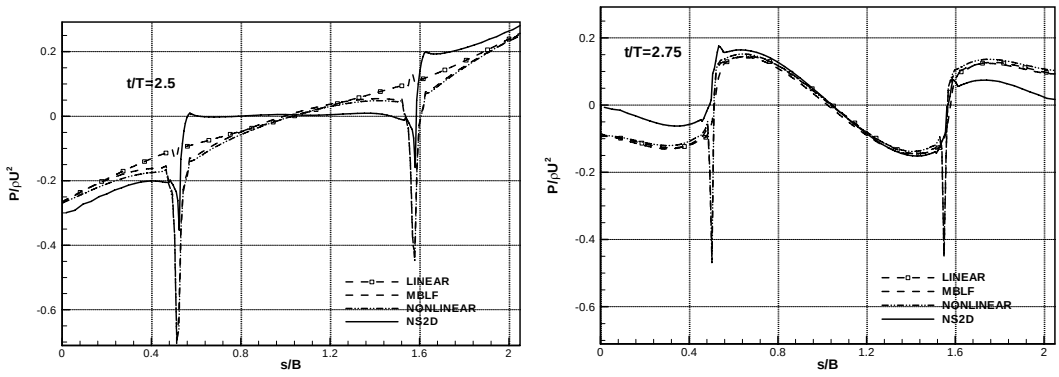

Figure 5.13: Pressure distributions on the hull at t/T=2.5 and t/T=2.75 (4% bilge keels and Fn=0.8).

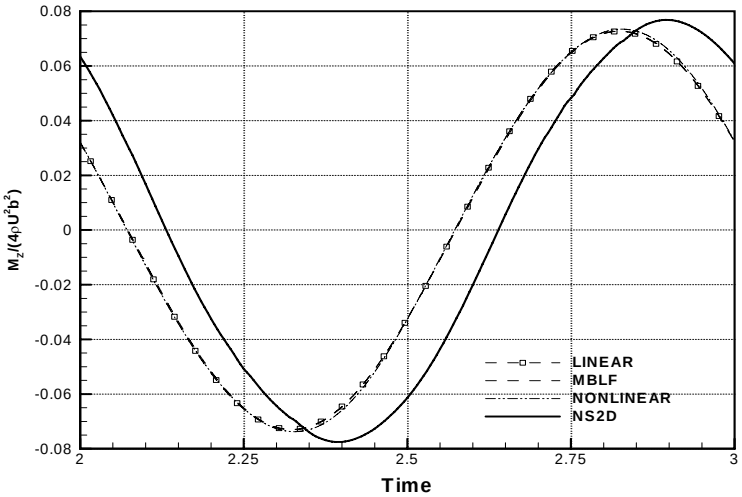

Figure 5.14: Moment histories from the viscous solver and the potential solver (4% bilge keels and Fn=0.8).

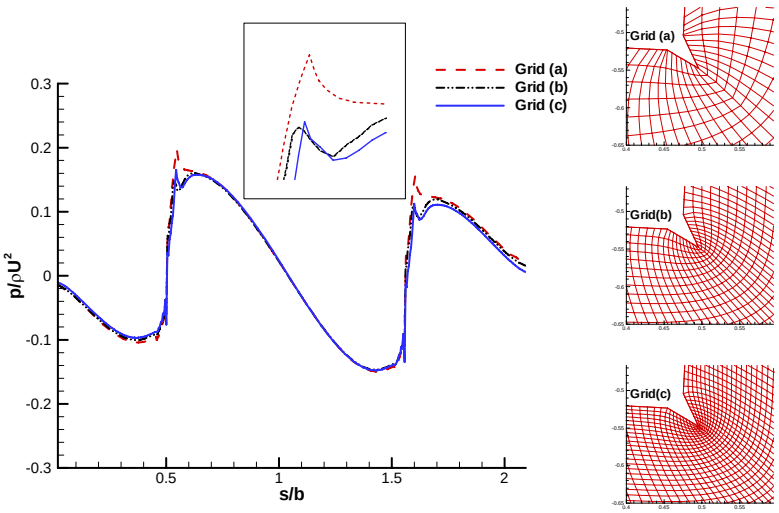

Figure 5.15: The pressure distribution along the FPSO hull from the present viscous solver for varying grid sizes and time step sizes at t/T=0.5 with Fn=0.8.

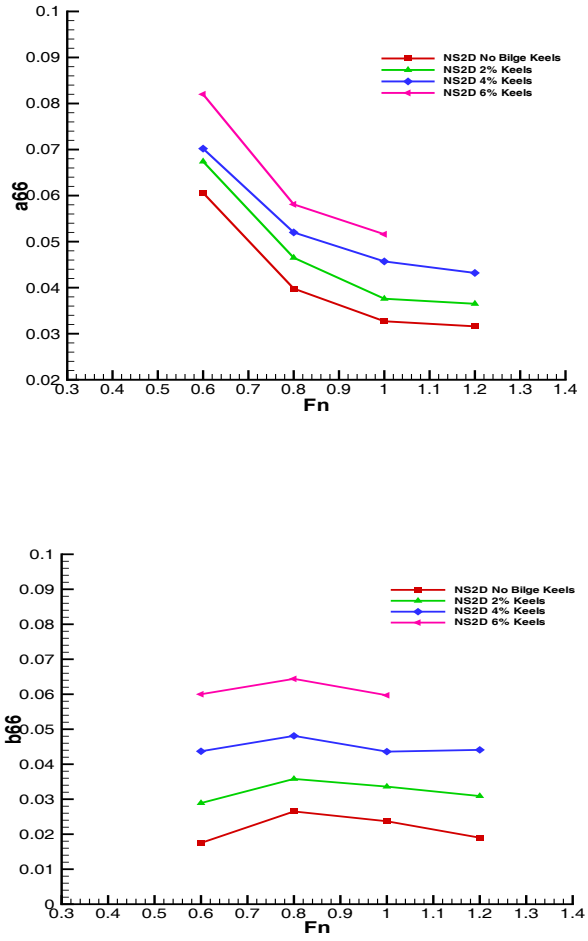

Figure 5.16: Effect of bilge keel length on predicted added mass (left) and damping (right) coefficients in roll for FPSO hull section.

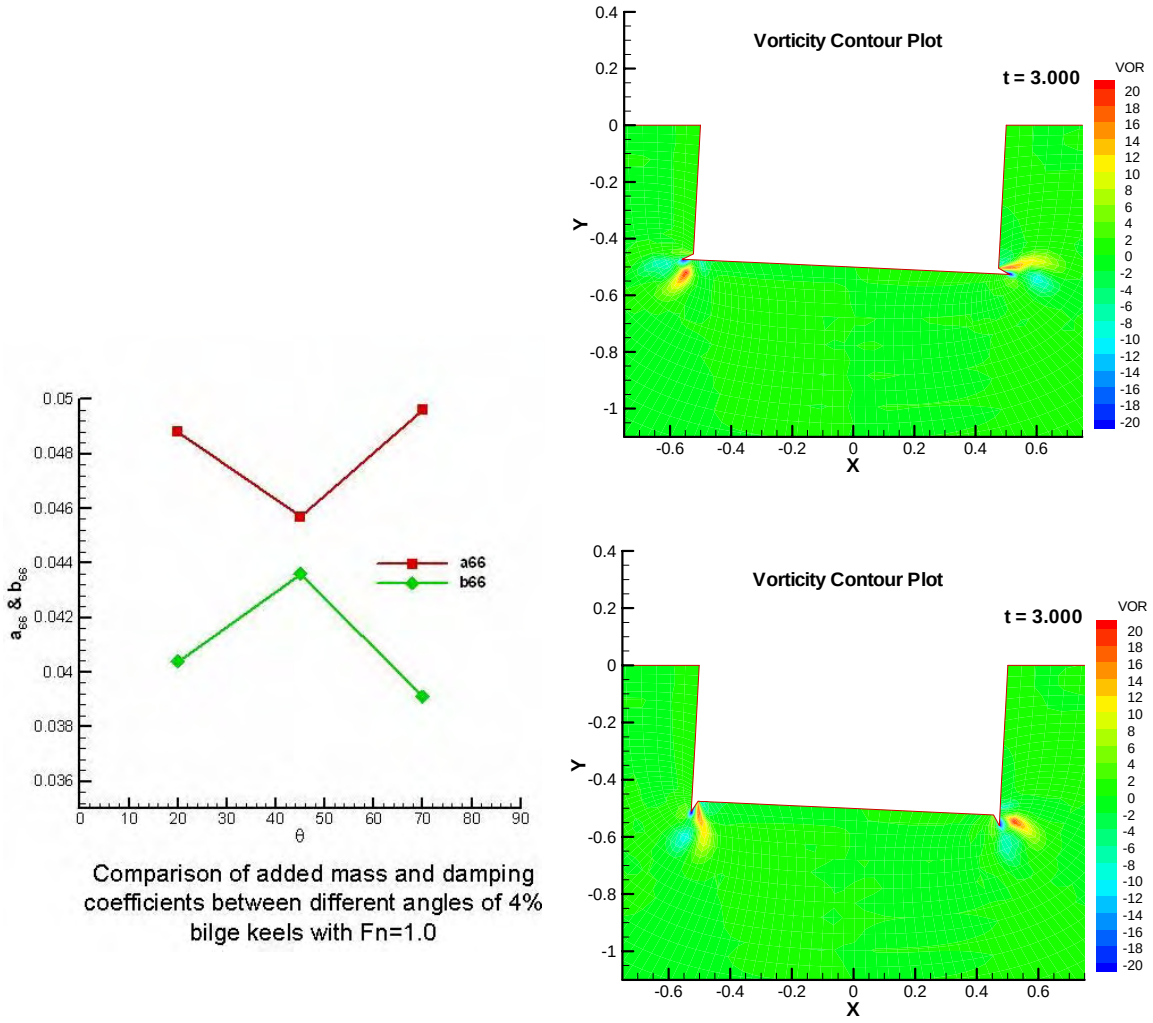

Figure 5.17: Effect of bilge keel orientation on results; hydrodynamic coefficients in roll (left), and vorticity contours (right)

6. Benefits to Sponsors:

A robust computational method for the hydrodynamic analysis of FPSO hull sections with bilge keels subject to roll or heave (also applicable in the case of sway) motions have been developed under this contract. The results of this method have been verified via exhaustive grid dependence studies and via comparisons with those of other methods, and validated via comparisons with measurements. The effects of viscosity have been found to be significant and classical linear theory has been found to be inadequate to predict the correct pressure distribution along the hull. The method can be applied, using strip theory, to provide the hydrodynamic coefficients of an actual FPSO hull, and thus help determine the effects of the bilge keel length, orientation, and extent along the hull, on the predicted motions for a given wave environment. The method in principle can be extended to three dimensions, even though this would require computer intensive calculations (which could be accelerated via parallel processing). The method can also be extended to analyze wave flows in confined domains (e.g. sloshing).

Publications and Theses Produced Under this MMS Contract:

1. Kinnas, S.A., Vinayan, V, *A BEM for the propagation of Nonlinear Free-surface waves, BeTeQ'05,* 6th International Conference on Boundary Element Techniques, Montreal, Canada, July 2005.

2. Vinayan, V., Kinnas, S.A., Yu, Y.-H., *Modeling of the Flow Around FPSO Hull Sections to Roll Motions: Effects of Non-linear Boundary Conditions,* OMAE 2005.

3. Yu, Y.-H., Kinnas, S.A., Vinayan, V., Kacham, K., *Modeling of Flow around FPSO Hull Sections Subject to Roll Motions: Effect of the Separated Flow around Bilge Keels,* ISOPE 2005.

4. Kacham, B., *Inviscid and Viscous 2D Unsteady Flow Solvers Applied to FPSO Hull Roll Motions,* MS thesis, UT Austin, Ocean Engineering Group, Department of Civil Engineering, December 2004 (also UT-OE Report 04-7)

5. Kinnas, S.A., Yu, Y.-H., Lee, H., Kakar, K., *Modeling of Oscillating Flow Past a Vertical Plate*, The 13th International Offshore and Polar Engineering Conference, Honolulu, Hawaii, May 25-30, 2003, pp.218-226.

6. Kinnas, S.A., Yu, Y.-H., Kacham, B., Lee, H., *A Model of the Flow around Bilge Keels of FPSO Hull Sections subject to Roll Motions*, The 12th Offshore Symposium, Texas Section of SNAME, Houston, TX, February 19, 2003.

7. Kakar, K., *Computational Modeling of FPSO Hull Roll Motions and Two-component Marine Propulsion Systems* , MS thesis, UT Austin, Ocean Engineering Group, Department of Civil Engineering, August 2002 (also UT-OE Report 02-3).

Related Publications and References:

- Choi, J.-K. and Kinnas, S.A., *An Unsteady 3-D Euler Solver Coupled with a Cavitating Propeller Analysis Method*, Twenty-third Symposium on Naval Hydrodynamics, Val de Reuil, France, September 17-22, 2000.
- Choi, J.-K. *Vortical Inflow – Propeller Interaction Using an Unsteady Three-Dimensional Euler Solver*, PhD thesis, Ocean Engineering Group, Department of Civil Engineering, The University of Texas at Austin, August 2000.
- Choi, J.-K. and Kinnas, S.A., *Prediction of Unsteady Effective Wake by a Euler Solver/Vortex-Lattice Coupled Method*, Journal of Ship Research, Vol. 47, pp. 131-144, June 2003.
- Yu, Y.-H., Kinnas, S.A., Vinayan, V., Kacham, K., *Modeling of Flow around FPSO Hull Sections Subject to Roll Motions: Effect of the Separated Flow around Bilge Keels*, ISOPE 2005.
- Vinayan, V., Kinnas, S.A., Yu, Y.-H., *Modeling of the Flow Around FPSO Hull Sections to Roll Motions: Effects of Non-linear Boundary Conditions*, OMAE 2005.
- Kacham, B., *Inviscid and Viscous 2D Unsteady Flow Solvers Applied to FPSO Hull Roll Motions*, MS thesis, UT Austin, Ocean Engineering Group, Department of Civil Engineering, December 2004 (also UT-OE Report 04-7) .
- Kinnas, S.A., Yu, Y.-H., Lee, H., Kakar, K., *Modeling of Oscillating Flow Past a Vertical Plate*, The 13th International Offshore and Polar Engineering Conference, Honolulu, Hawaii, May 25-30, 2003, pp.218-226.
- Kinnas, S.A., Yu, Y.-H., Kacham, B., Lee, H., *A Model of the Flow around Bilge Keels of FPSO Hull Sections subject to Roll Motions*, The 12th Offshore Symposium, Texas Section of SNAME, Houston, TX, February 19, 2003.
- Kinnas, S.A., Vinayan, V, *A BEM for the propagation of Nonlinear Free-surface waves*, 6th International Conference on Boundary Element Techniques, Montreal, Canada, July 2005.
- Kakar, K., *Computational Modeling of FPSO Hull Roll Motions and Two-component Marine Propulsion Systems* , MS thesis, UT Austin, Ocean Engineering Group, Department of Civil Engineering, August 2002 (also UT-OE Report 02-3).
- Na, J. H., Lee, W. C., Shin, S. S., and Park, I. K., *A Design of Bilge Keels for Harsh Environment FPSOs*, Proc 12th Int Offshore and Polar Eng Conf, Kitakyushu, Japan, ISOPE, Vol. 1, pp. 114-117, 2002.
- Sarpkaya, T. and O'Keefe, J. (1995). *Oscillating flow about two and three dimensional bilge keels*. In Proceedings of the 14th International Conference on Offshore Mechanics and Arctic Engineering, pages pp. 263-270, Copenhagen, Denmark.
- Seah, R. K. M. and Yeung, R. W., *Sway and Roll Hydrodynamics of Cylindrical Sections*, International Journal of Offshore and Polar Engineering, Vol. 13, No. 4, pp. 241-248, December 2003.
- Vugts, J. *The hydrodynamic coefficients for swaying, heaving and rolling cylinders in a free surface*, In International Shipbuilding Progress, pp. 251-276, 1968.
- Yeung, RW, Liao, SW, and Roddier, D. "Hydrodynamic Coefficients of Rolling Rectangular Cylinders", *Int J Offshore and Polar Eng*, vol. 8, No. 4., pp. 241-250, 1998.
- Yeung, RW, Roddier, D, Liao, S-W, Alessandrini, B, and Gentaz, L. "On roll hydrodynamics of cylinders fitted with bilge keels, " *Proc 23rd Symp on Naval Hydrodyn*, Val de Reuil, France, pp 863-880, 2001.
- Yeung, RW, and Vaidhyanathan, M. "Highly separated flow near a free surface." *Proc Int Conf on Hydrodyn*, Wuxi, China, pp 118-128, 1994.
- Young, Y.L and Kinnas, S.A., *A BEM Technique for the Modeling of Super-cavitating and Surface-Piercing Propeller Flows*, 24th Symposium on Naval Hydrodynamics, Fukuoka, JAPAN, 8-13 July, 2002.
- Young, Y.L., *Numerical Modeling of Supercavitating and Surface-Piercing Propellers*, PhD thesis, UT Austin, Ocean Engineering Group, Department of Civil Engineering, May 2002 (also UT-OE Report 02-1).

Appendix A: Formulation and Numerical Implementation of the Present Finite Volume Method

• Governing Equations

The vector formulations of the continuity equation and Navier-Stokes equations are written as

$$\begin{aligned} &\nabla \cdot \vec{U} = 0, \\ &\frac{\partial \vec{U}}{\partial t} + \vec{U} \cdot \nabla \vec{U} = -\frac{1}{\rho}\nabla p + \vec{f} + \nu \nabla^2 \vec{U}, \end{aligned} \tag{A.1}$$

where ν is the kinematic viscosity; $\vec{U}$ is the total velocity vector; $\vec{f}$ is the body force per unit mass; ρ is the density of the fluid; p represents pressure; and t indicates time. The partial differential equations are solved by coupling the continuity equations and Navier-Stokes equations based on the primitive variable method. [Note that the in the code, the above equations are non-dimensionalized with respect to a length scale B (the breadth of the hull), a time scale T (the period of oscillation), velocity scale B/T].

• Cell Based Finite Volume Method

A semi-discrete integral formulation of the momentum equation can be given as

$$\begin{aligned} &\frac{\partial u_{i,j}}{\partial t} A_{i,j} + \sum_{faces} \left(u_{i,j} V_n - \nu \frac{\partial u_{i,j}}{\partial n} \right) ds_{face} = -\sum_{faces} p_{i,j} dy, \\ &\frac{\partial v_{i,j}}{\partial t} A_{i,j} + \sum_{faces} \left(v_{i,j} V_n - \nu \frac{\partial v_{i,j}}{\partial n} \right) ds_{face} = -\sum_{faces} p_{i,j} dx, \end{aligned} \tag{A.2}$$

where $A_{i,j}$ is the area of the cell; ds_{face} is the length of each cell face; dx and dy represent the horizontal and vertical length of each cell face.

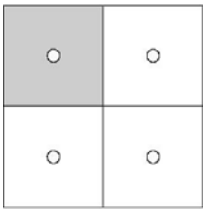

• Upwind scheme (QUICK)

It uses a three-point upstream-weighted quadratic interpolation for the cell face value, while calculating the flux.

• Time Marching (Three Time Level Method)

$$\vec{U}^{n+1} = \frac{4}{3}\vec{U}^{n} - \frac{1}{3}\vec{U}^{n-1} + \frac{2\Delta t}{3} f^{n+1} \tag{A.3}$$

where f represents the summation of the convective terms, the viscous terms and the pressure terms at time step n+1.

• Pressure-correction Method
(SIMPLE Method, Patankar 1980)

$$\begin{aligned} &p = p^{*} + p', \\ &v_n = v_n^{*} + v_n' = v_n^{*} - \Delta t \frac{\partial p'}{\partial n}, \end{aligned} \tag{A.4}$$

where ' ' ' indicates the correction terms; v_n represents the corrected normal velocity on the cell face; v_n^* is the normal velocity without considering the correction term, and p^* indicates the value of pressure from previous iteration.
In order to satisfy the continuity equation, $\Sigma_{face}\, v_n\, ds_{face}=0$, the pressure-correction term can be solved as

$$\sum_{face} \Delta t \frac{\partial p'}{\partial n} ds_{face} = \sum_{face} v_n^* ds_{face}. \tag{A.5}$$

In order to avoid the checkerboard oscillation problem, two additional terms are added to the average normal velocity as follows

$$v_n^* = v_{av}^* + \Delta t \left(\frac{1}{a_{i,j}} \frac{\partial p^*}{\partial n}\bigg|_{av} - \frac{1}{a_{i,j}} \frac{\partial p^*}{\partial n}\bigg|_{d} \right), \tag{A.6}$$

where $a_{i,j}$ represents the coefficient of the unknown velocity in the momentum equation; *av* indicates the value obtained from the interpolation of the cell center value; *d* represents the value calculated directly at the cell face center, and v_{av}^* represents the average normal velocity on the cell face which is also interpolated from the cell center velocities.

• Moving grid
Under roll motion, the FPSO hull is forced to rotate periodically. Therefore, the grids are required to move along with the body near the FPSO hull. For calculating the time derivative term, additional terms need to be taken into account. It can be expressed as

$$\frac{\partial \zeta}{\partial t} = \frac{\Delta \zeta}{\Delta t} - u_{grid}\left(\frac{\partial \zeta}{\partial x}\right) - v_{grid}\left(\frac{\partial \zeta}{\partial y}\right), \tag{A.7}$$

where ζ can be any variable (u, v, or p); $\Delta\zeta/\Delta t$ represents the total change in the value of ζ with both increments in time and the corresponding change in the location of the point; u_{grid} and v_{grid} are the velocities of the moving grid.

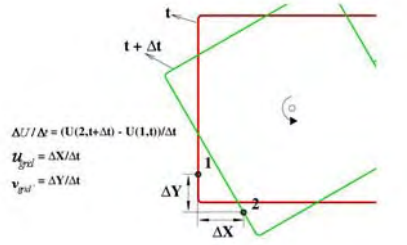

• Grid orientation
In order to have a better grid geometry near the sharp edge, the grid orientation is changed from i,j indexing to global indexing.

(a) i,j indexing

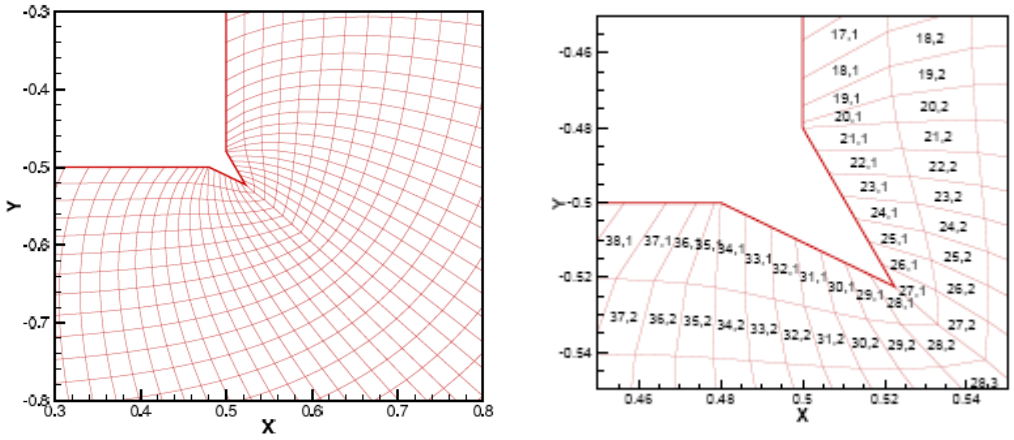

(b) Global indexing

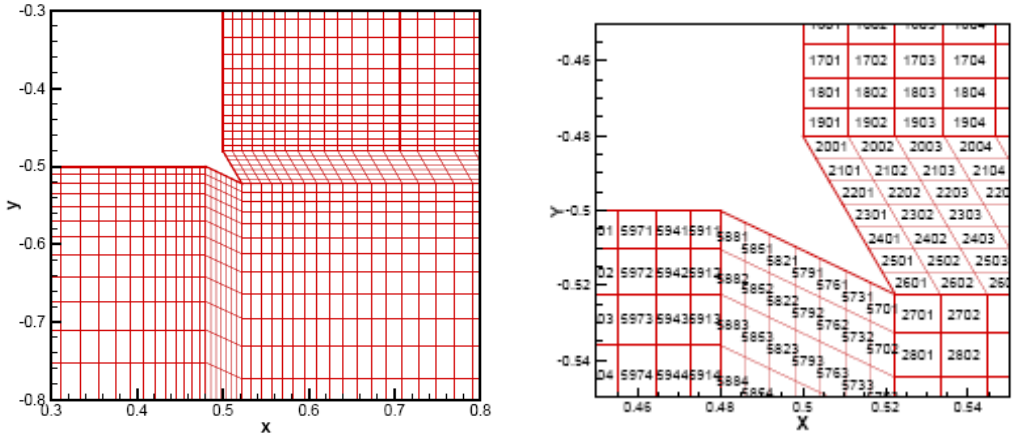

Fig A.1: Grid indexing, (a) i,j indexing, (b) global indexing.

• Boundary Conditions of the Roll Motion

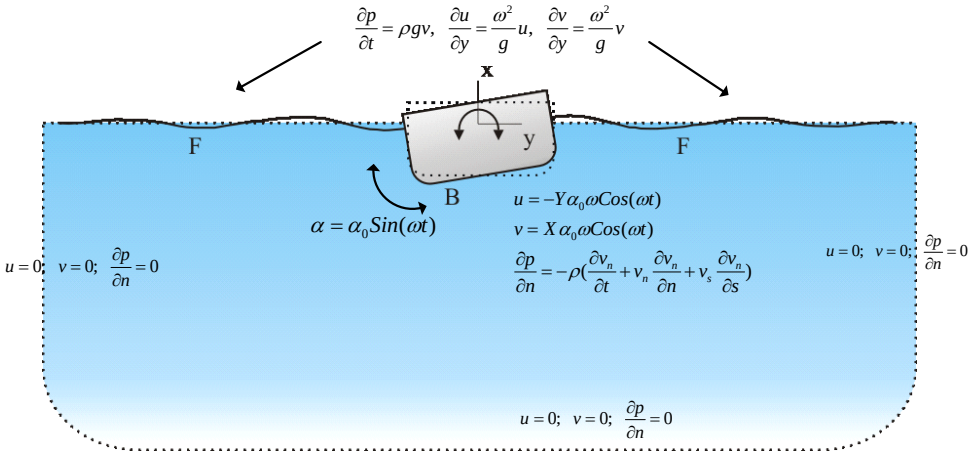

Fig A.2: Boundary conditions and flow domain.

Boundary Conditions on the Hull

Kinematic and no-slip boundary conditions are applied on the hull so that the fluid particle velocities are consistent with the hull velocities. The roll angle, the angular velocity, and the velocity magnitude are defined as follows:

$$\begin{aligned} \alpha &= \alpha_0 Cos(\omega t), \\ \dot{\alpha} &= -\alpha_0 \omega Sin(\omega t), \\ q &= -r\alpha_0 \omega Sin(\omega t), \end{aligned} \tag{A.8}$$

where α is the roll angle; $\dot{\alpha}$ is the angular velocity, q is the total velocity of the point being considered on the hull, r is the distance of the point on the hull to the center of the roll motion, α_0 is the amplitude of roll and ω represents the angular frequency of roll motion.

The corresponding velocities and normal derivative of pressure on the instantaneous hull boundary are specified as

$$\begin{aligned} u &= -Y\alpha_0 \omega Sin(\omega t), \\ v &= X\alpha_0 \omega Sin(\omega t), \\ \frac{\partial p}{\partial n} &= -\rho\left(\frac{\partial v_n}{\partial t} + v_n \frac{\partial v_n}{\partial n} + v_s \frac{\partial v_n}{\partial s}\right), \end{aligned} \tag{A.9}$$

where X and Y are the horizontal and vertical components of the position vector, $X^2+Y^2=r^2$; u and v are the velocity components in the horizontal and vertical directions; n and s indicate the normal and tangential directions of the boundaries; v_n and v_s are the corresponding velocities in n and s directions.

Boundary Conditions on Far Boundaries

The outflow boundaries and the bottom boundary are assumed to be far enough for the waves not to disturb the fluid particles at the boundaries, and the pressure derivative with respect to the normal direction is equal to zero.

$$u = 0; \quad v = 0; \quad \frac{\partial p}{\partial n} = 0. \tag{A.10}$$

Free Surface Boundary Conditions

Linearized free surface boundary conditions are applied in this 2-D Navier-Stokes solver. The Kinematic Free Surface Boundary Condition (KSFBC) and the Dynamic Free Surface Boundary Condition (DSFBC are combined into

$$\frac{\partial p}{\partial t} = \rho g v\,, \tag{A.11}$$

and the boundary conditions of the velocities can be given as

$$\frac{\partial u}{\partial y} = \frac{\omega^2}{g} u, \quad \frac{\partial v}{\partial y} = \frac{\omega^2}{g} v, \tag{A.12}$$

where g is acceleration due to gravity.

Appendix B: Formulation and Numerical Implementation of the Boundary Element Method

• Governing Equation

The flow is described by a velocity potential φ(x,t) which satisfies the Laplace equation

$$\nabla^2\varphi(x,t) = 0; \quad x \in \Omega(t) \tag{B.1}$$

where t is the time and Ω(t) represents the fluid domain as shown in Fig B.1. Figure B.1 also shows the boundaries of the fluid domain Ω(t): F(t) and B(t) represent the instantaneous positions of the free-surface and hull surface respectively, Σ represents the far-field boundary used to truncate the infinite domain into a finite one but placed far enough from the body to avoid reflection of waves.

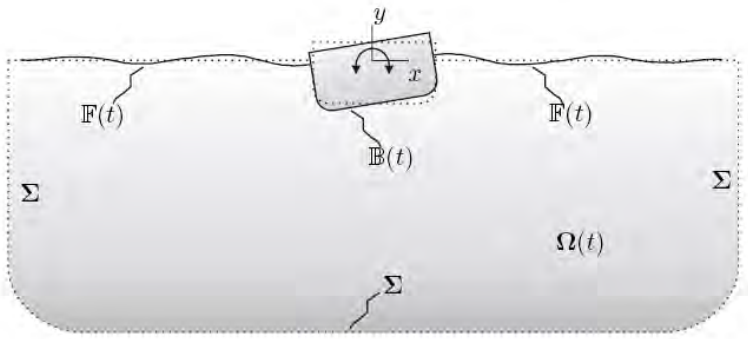

Fig B.1: FLUID DOMAIN AND CORRESPONDING BOUNDARIES

• Boundary Conditions

Fully nonlinear boundary conditions are imposed on the free-surface F(t). The dynamic boundary condition (DFSBC) in the Lagrangian form is

$$\frac{D\varphi}{Dt} = \frac{1}{2}|\nabla\varphi|^2 - g\eta - \mathrm{P_F} \tag{B.2}$$

satisfied on the exact free-surface. In Eq.(B.2), $[D/Dt] \equiv [(\partial)/(\partial t)]+\nabla\varphi\cdot\nabla$ denotes the material derivative, $\eta \equiv \eta(x,t)$ the instantaneous free-surface and P_F the pressure on the free-surface assumed to be zero.

An equally important free-surface boundary condition is the kinematic boundary condition (KFSBC) also represented in the Lagrangian form as

$$\frac{D\mathbf{x}}{Dt} = |\nabla\varphi|; \mathbf{x} \in \mathbf{F}(t) \tag{B.3}$$

On the body surface B(t),

$$\varphi_n = V(x,t)\cdot n; \quad x,n \in B(t) \tag{B.4}$$

where, $\varphi_n=\nabla\varphi\cdot n$ is the normal fluid velocity, n the unit surface normal and V(x,t) the prescribed motion of the hull. In the case of roll, the hull is subject to a forced sinusoidal angular motion of

the form

$$\alpha = \alpha_0 \sin(\omega t) \tag{B.5}$$

where α_0 is the amplitude of roll motion and ω the corresponding circular frequency. In terms of the Cartesian components, the prescribed roll motion is

$$V(x,t)=(-y\ \dot{\alpha}\ ,x\ \dot{\alpha}\ ) \tag{B.6}$$

The far-field boundary Σ is assumed to be a no-flux surface and the corresponding boundary condition is

$$\nabla\varphi \cdot n=0;\quad x,n \in \Sigma \tag{B.7}$$

Special attention is paid to place the boundary far away from the body to avoid reflection of the waves generated by the hull motion.

Boundary Integral Equation

The BVP for the velocity potential is converted into a Boundary Integral Equation (BIE) by introducing a Green's function $G(p,q)=\ln r_{pq}$ (satisfies the Laplace equation), where $r_{pq}=|p-q|$, $p \equiv p(x)$ is the field point and $q \equiv q(x)$ is the source point. The BIE obtained by applying Green's third identity to $\varphi(x,t)$ and $G(p,q)$ is

$$\alpha(p)\varphi(p) + \int_{\Gamma} \varphi(q) \frac{\partial G(p,q)}{\partial n(q)} d\Gamma_q = \int_{\Gamma} G(p,q) \frac{\partial \varphi(q)}{\partial n(q)} d\Gamma_q \tag{B.8}$$

where $p \in \Gamma$ and Γ represents the boundary of the fluid domain ($\Gamma \equiv F \cup B \cup \Sigma$), $\alpha(p)$ is a solid angle ($\alpha = 0.5$ when the singularities are on the boundary).

MEL Approach

The MEL approach can be traced back to the work by Longuet-Higgins and Cokelet in the numerical simulation of non-linear waves. At any given time t, the MEL approach basically involves two steps:

1. Given $\mathbf{B}(t)$,$\varphi_n(\mathbf{B})$,$\mathbf{F}(t)$ and $\varphi(\mathbf{F})$, the BIE is solved to obtain $\varphi_n(\mathbf{F})$ and in turn $\nabla\varphi(\mathbf{F})=(\varphi_x,\varphi_y)$. The solution of the BIE is completely defined in terms of the values at the domain boundaries.
2. Time-integration of the kinematic and dynamic free-surface boundary conditions to update the geometry and potential of the free-surface.

The above process is repeated over time to advance the solution.

Initial Conditions

At time t=0, the following conditions are imposed on the free-surface

$$\left.\begin{aligned} \varphi(x,0) &= 0 \\ \eta(x,0) &= 0 \end{aligned}\right\} \ x \in F(t) \tag{B.9}$$

A ramp function is used to gradually increase the amplitude of motion of the hull to prevent any transient waves associated with an impulsive start. The function is applied over one period and

has the form

$$R(t)=\frac{1}{2}\left(1-\cos\frac{\pi t}{T}\right) \quad ;t \le T$$
$$R(t)=1 \quad ;t>T \tag{B.10}$$

Forces and Moments on the Hull

The nonlinear hydrodynamic pressure on the hull can be evaluated using the Bernoulli's equation

$$\frac{P}{\rho}=-\frac{\partial\varphi}{\partial t}-\frac{1}{2}|\nabla\varphi|^2 \tag{B.11}$$

However, on the body, a semi-Lagrangian approach is used to update the geometry and requires the inclusion of additional terms in Eq. (B.11) . The modified form of Eq. (B.11) is

$$\frac{P}{\rho}=-\frac{\delta\varphi}{\delta t}-\frac{1}{2}|\nabla\varphi|^2+\nabla\varphi.\mathbf{V}_g \tag{B.12}$$

where V_g is the grid/node velocity and the operator $[(\delta)/(\delta t)] \equiv [(\partial)/(\partial t)]+V_g\cdot\nabla$.

The instantaneous forces (F) and moments (M) on the hull are evaluated by integrating the hydrodynamic pressure on the wetted portion of the body surface.

$$\mathbf{F} = -\int_{B(t)} P\mathbf{n}\,d\Gamma \qquad \mathbf{M} = -\int_{B(t)} P\,\mathbf{r}\times\mathbf{n}\,d\Gamma \tag{B.13}$$

with the roll moment being,

$$\mathbf{M_z} = -\int_{B(t)} P(xn_y - yn_x)d\Gamma \tag{B.14}$$

where $n=(n_x,n_y)$ is the normal to the hull surface and $x=(x,y)$ the position vector of a point on the body.

For roll, according to linear potential theory, the hydrodynamic moment in Eq.(B.14) can be written as a linear combination of added-mass (inertia) and damping components.

$$M_z(t) = -a_{66}\,\ddot{\alpha} - b_{66}\,\dot{\alpha} \tag{B.15}$$

where a_{66} is the roll added-mass coefficient, b_{66} the damping coefficient, $\dot{\alpha}$ and $\ddot{\alpha}$ are the angular velocity and acceleration respectively (time derivatives of roll angular motion in Eq. (5)). The hydrodynamic coefficients are evaluated by extracting the Fourier coefficients of the primary frequency over a period.

• ***Numerical Formulation***

The two important aspects that dominate the numerical formulation of the problem are 1) the solution of the boundary integral equation and 2) the time integration of the free-surface boundary conditions.

Discretization of BIE

In this model, the BIE is approximated using constant strength elements with the computational nodes at the mid-point of each panel/element. With this approximation, Eq. (B.8) reduces to the form

$$\frac{1}{2}\varphi_i + \sum_{j=1}^{N}\left(\int_{\Gamma_j}\frac{\partial G_{ij}}{\partial n}d\Gamma\right)\varphi_j = \sum_{j=1}^{N}\left(\int_{\Gamma_j} G_{ij}d\Gamma\right)\varphi_{nj} \qquad \text{(B.16)}$$

The discretized form in Eq. (B.16) can be expressed in a matrix form as

$$[A][\varphi]=[B][\varphi_n] \qquad \text{(B.17)}$$

where [A] and [B] are the influence coefficient matrices. Exact analytical expressions of the integrals in Eq. (B.16) are used to evaluate the influence coefficients.

However, in order to obtain a solution, the matrix form of the BIE has to be rearranged to account for the known and unknown values on each of the boundary surface. The rearranged form of the equation can be written as:

$$\tilde{[A]}\begin{Bmatrix}(\varphi_n)_F\\ \varphi_B\\ \varphi_\Sigma\end{Bmatrix} = \tilde{[B]}\begin{Bmatrix}\varphi_F\\ (\varphi_n)_B\\ (\varphi_n)_\Sigma\end{Bmatrix}$$

or

$$\tilde{[A]}[X] = [F] \qquad \text{(B.18)}$$

Time Integration

A strictly Lagrangian approach is used for the time-integration of the free-surface kinematic and dynamic boundary conditions. An alternative approach would be a semi-Lagrangian approach which results in a more complicated set of boundary conditions.

The free-surface boundary conditions Eqs. (B.2)- (B.3) are of the general form

$$\frac{DY}{Dt} = f(t,Y) \qquad \text{(B.19)}$$

where, Y can be either x or φ. A fourth-order Runge-Kutta scheme, as shown below, is used to integrate Eq. (B.19) in time.

$$\begin{aligned} k_1 &= \Delta t \quad f(t_i, Y_i)\\ k_2 &= \Delta t \quad f(t_i+0.5\Delta t, Y_i+0.5\,k_1)\\ k_3 &= \Delta t \quad f(t_i+0.5\Delta t, Y_i+0.5\,k_2)\\ k_4 &= \Delta t \quad f(t_{i+1}, Y_i+k_3)\\ Y_{i+1} &= Y_i + (k_1+2k_2+2k_3+k_4)/6 \end{aligned} \qquad \text{(B.20)}$$

Evaluation of Pressure

The evaluation, to a sufficient level of accuracy, of the time derivative of the velocity potential and the node velocity in Eq. (B.12), is critical to obtaining the correct pressure on the hull. The pressure is evaluated from the expression

$$\frac{\delta f(t_0+\Delta t)}{\delta t} = \frac{1}{4\Delta t}\Big[-2f(t_0) - 4f^{(1)}(t_0+0.5\Delta t) \\ -4f^{(2)}(t_0+0.5\Delta t) + 10f(t_0+\Delta t)\Big] - \frac{1}{2}\frac{\delta f(t_0)}{\delta t} \tag{B.21}$$

where f can be either φ or x (V_g=(δx)/(δt). The scheme utilizes the mid-step values of the fourth-order Runge-Kutta scheme with superscripts $^{(1)}$ and $^{(2)}$ indicating the first and second mid-steps respectively.

Appendix C: Definitions of Parameters and Hydrodynamic Coefficients

• Definitions of Parameters

Three non-dimensional parameters are used in the FPSO hull roll motion problem and are defined as

$Fn_b = \omega\sqrt{b/g}$, Froude number,

$\mathrm{Re} = 4b^2\omega/2\pi\nu$, Reynolds number,

$\mathrm{KC}=\alpha_0\sqrt{2}b\cdot 2\pi/K_d$, Keulegan Carpenter number.

where *b* indicates the half beam.

• Hydrodynamic Coefficients

According to the linear potential theory, the uncoupled hydrodynamic moment can be written as a linear combination of the inertia and damping terms.

$$M_Z(t) = -\hat{a}_{66}\ddot{\alpha} - \hat{b}_{66}\dot{\alpha},$$

where M_Z is the moment which is a function of time; $\hat{a}_{66}$ is the roll added mass coefficient; $\hat{b}_{66}$ is the roll damping coefficient; $\ddot{\alpha}$ and $\dot{\alpha}$ represent the angular acceleration and velocity respectively.

The hydrodynamic coefficients for the primary frequency are extracted from the moment history by using Fourier analysis and the following expressions are obtained for the coefficients:

$$\hat{a}_{66} = \frac{1}{\pi\alpha_o\omega}\int_0^T M_Z(t)\sin(\omega t)dt,$$

$$\hat{b}_{66} = -\frac{1}{\pi\alpha_o}\int_0^T M_Z(t)\cos(\omega t)dt.$$

The above equations are non-dimensionalized by density, the draft and half-beam of hull.

$$a_{66} = \frac{\hat{a}_{66}}{8\rho d b^3},$$

$$b_{66} = \frac{\hat{b}_{66}}{8\rho d b^3}\sqrt{\frac{b}{g}},$$

where *d* is the draft of the hull.

Appendix D: Roll Response Amplitude Operator

EQUATION OF MOTION

The equation of motion for rolling can be expressed as

$$a\frac{d^2\varphi}{dt^2} + b\frac{d\varphi}{dt} + c\varphi = M_{\varphi} = M_0\cos(\omega_e t) \tag{1}$$

where,

a = total mass moment of inertia
b = damping moment coefficient
c = restoring moment coefficient
M_{φ} = exciting moment
ω_e = wave encountering frequency (2)

These coefficients together determine the complete roll motion of the vessel.

- ADDED MASS MOMENT OF INERTIA

The virtual mass moment of inertia for rolling is the moment of inertia of the actual mass of the vessel plus the added mass moment of inertia. Thus

$$a = I_{xx} + I'_{xx} \tag{3}$$

where, I_{xx} is the mass moment of inertia of the actual mass of the vessel. It is usually expressed in terms of the radius of gyration k_{xx} and the mass displacement of the vessel Δ.

$$I_{xx} = \Delta k_{xx}^2 \tag{4}$$

Also, the radius of gyration is expressed as a fraction of the breadth of the vessel B. Let $k_{xx} = rB$.

For the numerical experiments based on the two-dimensional hull sections, the added mass moment of inertia for rolling is expressed as follows:

$$a_{66} = \frac{\hat{a}_{66}}{\rho B^2 \forall} \tag{5}$$

where, for the two-dimensional hull-section

a_{66} = non–dimensional added mass moment of inertia
$\hat{a}_{66}$ = dimensional added mass moment of inertia
$\forall$ = cross–sectional area of hull–section (6)

Thus,

$$\begin{aligned} I'_{xx} &= a_{66} L \\ &= a_{66} \rho B^2 \forall L \\ &= a_{66} B^2 \Delta \end{aligned} \tag{7}$$

where, $\nabla = \forall L$ is the volume displacement of the vessel, $\Delta = \rho\nabla$ is the mass displacement of the vessel and L is the length of the vessel.

Thus,

$$\begin{aligned} a &= \Delta(k_{xx}^2 + a_{66}B^2) \\ &= \Delta B^2(a_{66} + r^2) \end{aligned} \tag{8}$$

$$a = \Delta B^2(a_{66} + r^2) \tag{9}$$

- DAMPING COEFFICIENT

For the numerical experiments based on the two-dimensional hull sections, the damping coefficient for rolling is expressed as follows:

$$b_{66} = \frac{\hat{b}_{66}}{\rho B^2 \forall} \sqrt{\frac{B}{2g}} \tag{10}$$

where, for the two-dimensional hull-section

$$\begin{aligned} b_{66} &= \text{non–dimensional dammping coefficient} \\ \hat{b}_{66} &= \text{dimensional damping coefficient} \\ \forall &= \text{cross–sectional area of hull–section} \end{aligned} \tag{11}$$

Thus,

$$b = b_{66} \Delta B^2 \sqrt{\frac{2g}{B}} \tag{12}$$

- RESTORING MOMENT COEFFICIENT

The restoring moment coefficient c can be derived using the wall-sided formula (for small angles of roll) and is as follows

$$c = \rho g \Delta \overline{GM}_T \tag{13}$$

where $\overline{GM}_T$ is the transverse metacentric height of the vessel.

- EXCITING MOMENT FOR ROLLING

For beam seas, the exciting moment can be expressed as

$$M_\phi = c\alpha_M \sin\omega_e t \tag{14}$$

where, α_M is the maximum slope of the wave.

Putting all the coefficients together, the solution to the equation of motion of roll can be written as

$$\varphi = e^{-\nu t}(C \cos\omega_d t + D \sin\omega_d t) + \varphi_a \sin(\omega_e t - \varepsilon_2) \tag{15}$$

where,

$$\begin{aligned}
\omega_d &= \sqrt{\omega_\phi^2 - \nu^2} \\
\frac{\varphi_a}{\alpha_M} &= \frac{1}{\sqrt{(1-\Lambda^2)^2 + 4\kappa^2\Lambda^2}} \\
\epsilon_2 &= \frac{2\kappa\Lambda}{1-\Lambda^2} \\
\nu &= \frac{b}{2a} \\
\omega_\varphi^2 &= \frac{c}{a} \\
\Lambda &= \frac{\omega_e}{\omega_\varphi}
\end{aligned}$$

ω_d	:	damped roll frequency
φ_a/α_M	:	Response amplitude operator
ε_2	:	phase angle (phase between response of hull and exciting moment)
ν	:	damping coefficient
ω_φ	:	roll frequency without damping
Λ	:	Tuning factor
κ	:	non-dimensional damping coefficient = ν/ω_φ

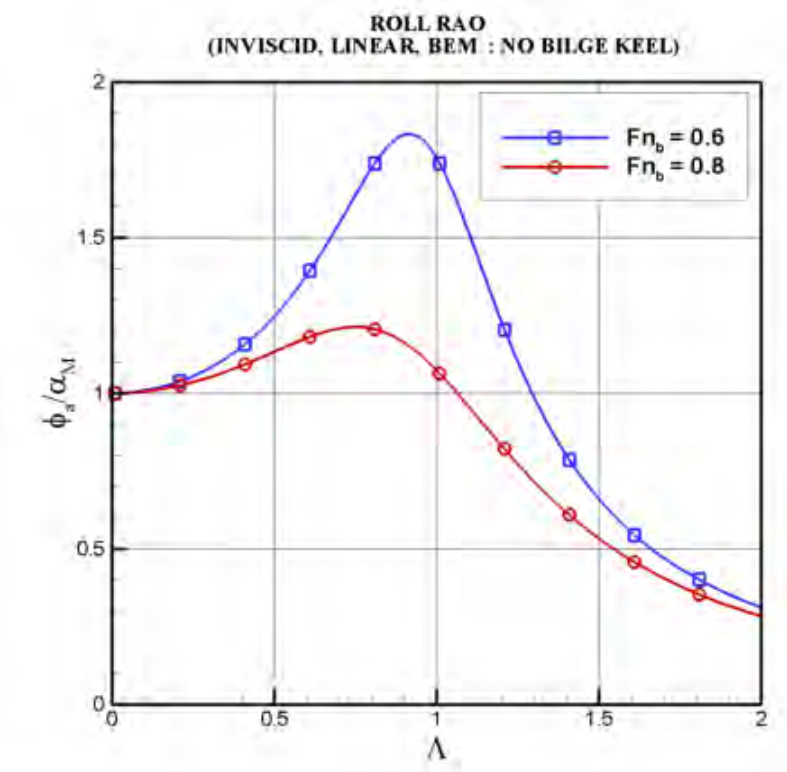

Figure D.1: Comparison of RAOs for Fn_b=0.6 and 0.8; Inviscid results with NO BILGE KEELS

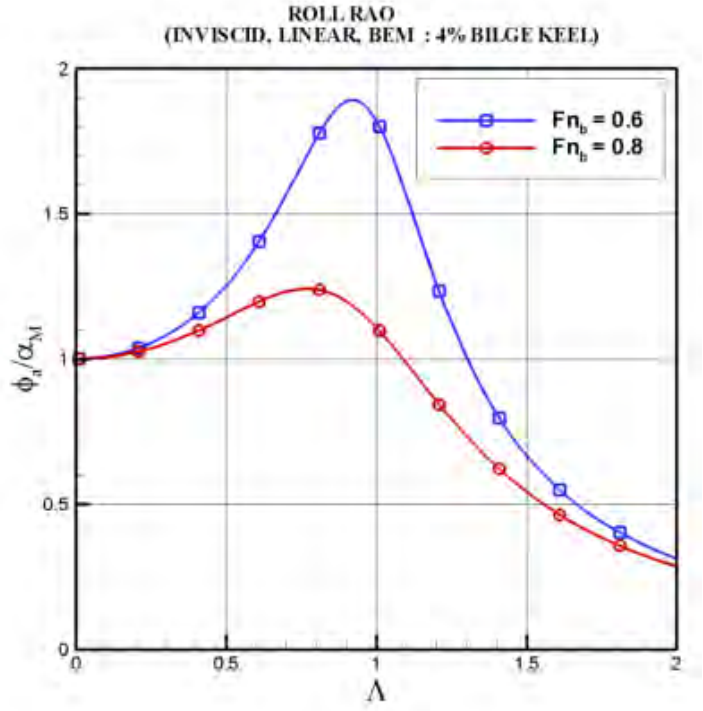

Figure D.2: Comparison of RAOs for Fn_b=0.6 and 0.8; Inviscid results with 4% BILGE KEELS

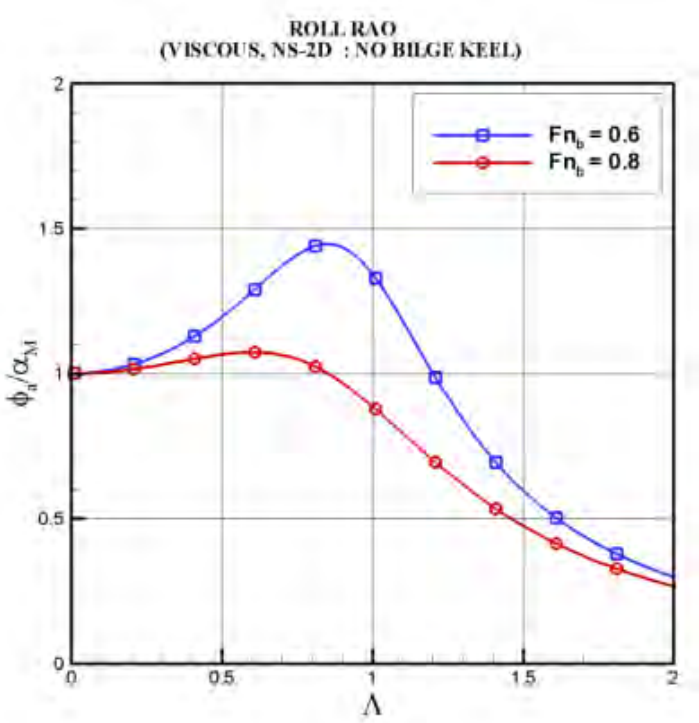

Figure D.3: Comparison of RAOs for Fn_b=0.6 and 0.8; Viscous results with NO BILGE KEELS

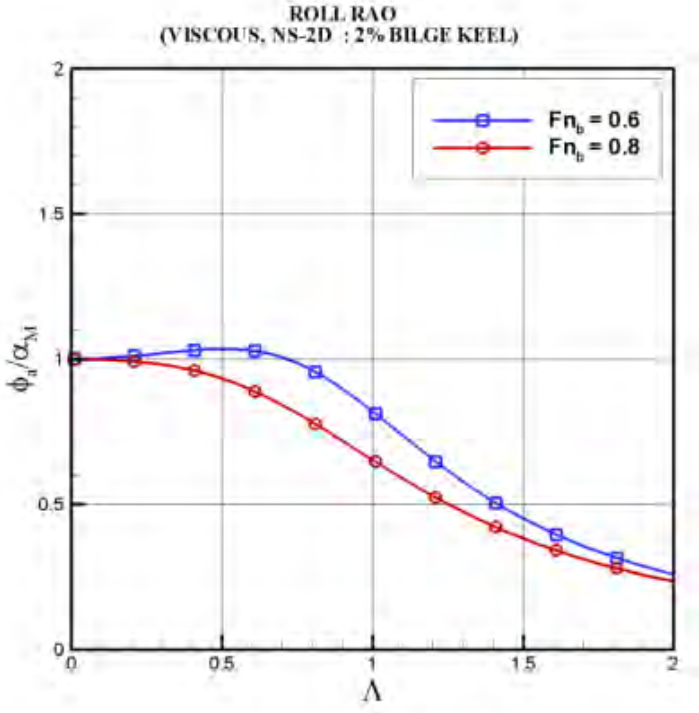

Figure D.4: Comparison of RAOs for Fn_b=0.6 and 0.8; Viscous results with 2% BILGE KEELS

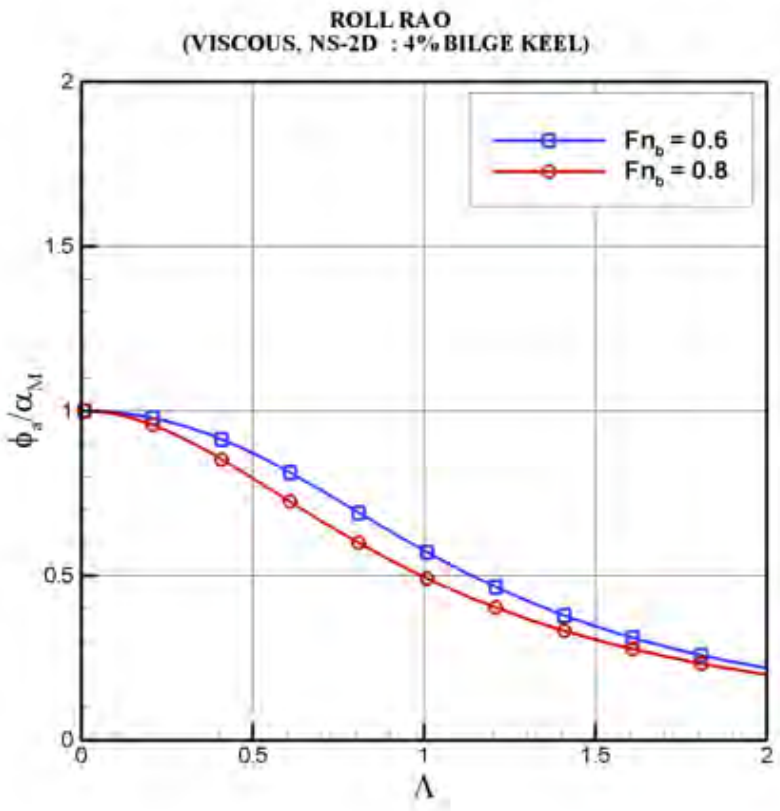

Figure D.5: Comparison of RAOs for Fn_b=0.6 and 0.8; Viscous results with 4% BILGE KEELS

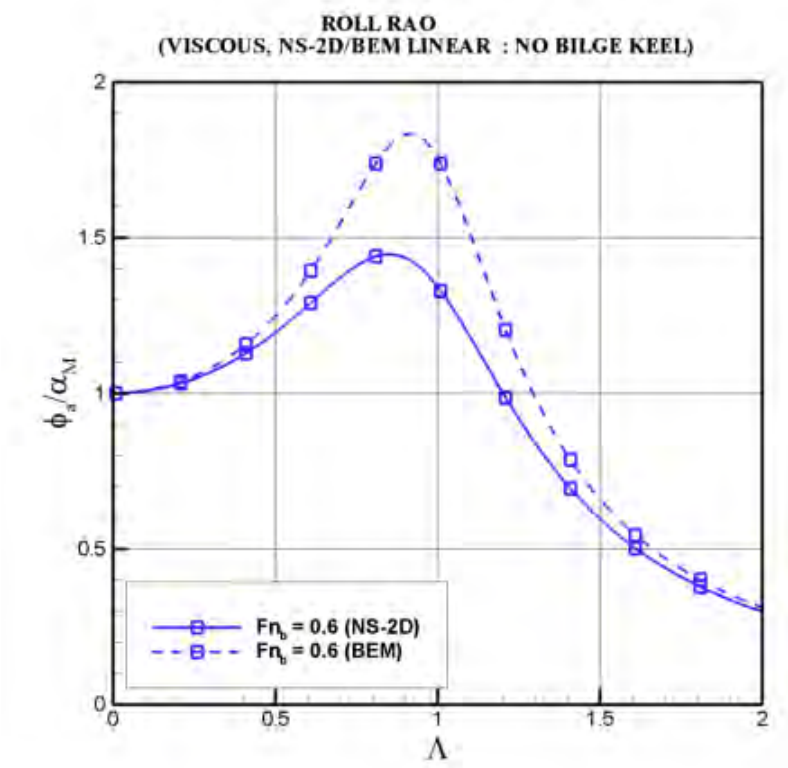

Figure D.6: Comparison of RAOs for Fn_b=0.6; Viscous and Inviscid results with NO BILGE KEELS

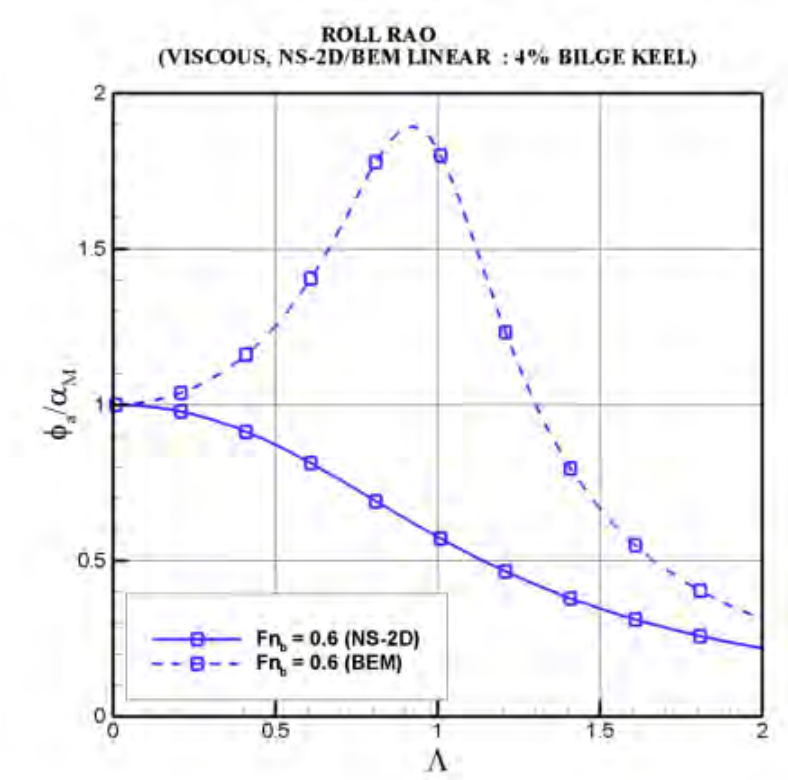

Figure D.7: Comparison of RAOs for Fn_b=0.6; Viscous and Inviscid results with 4% BILGE KEELS

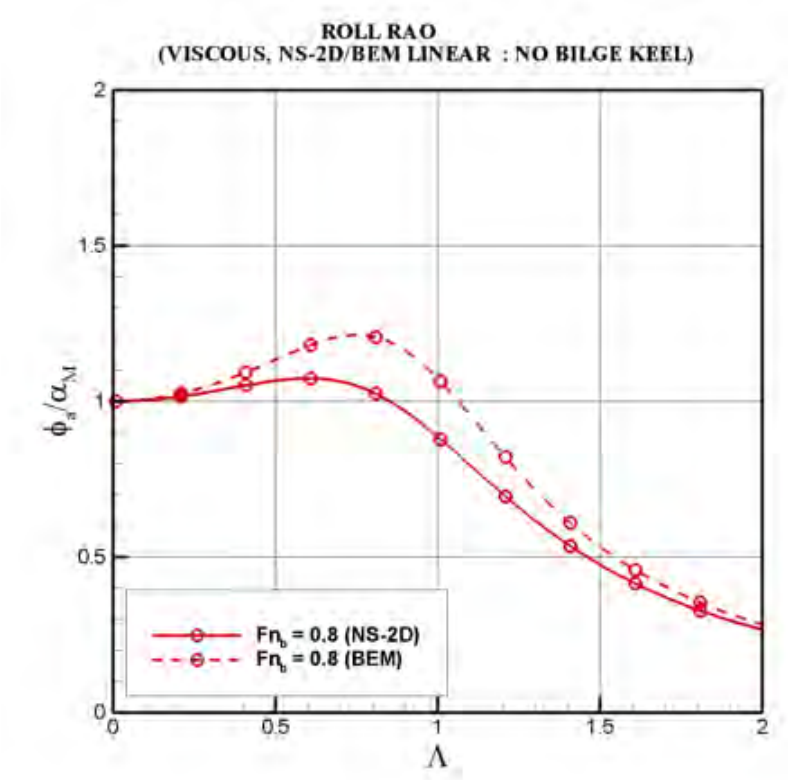

Figure D.8: Comparison of RAOs for Fn_b=0.8; Viscous and Inviscid results with NO BILGE KEELS

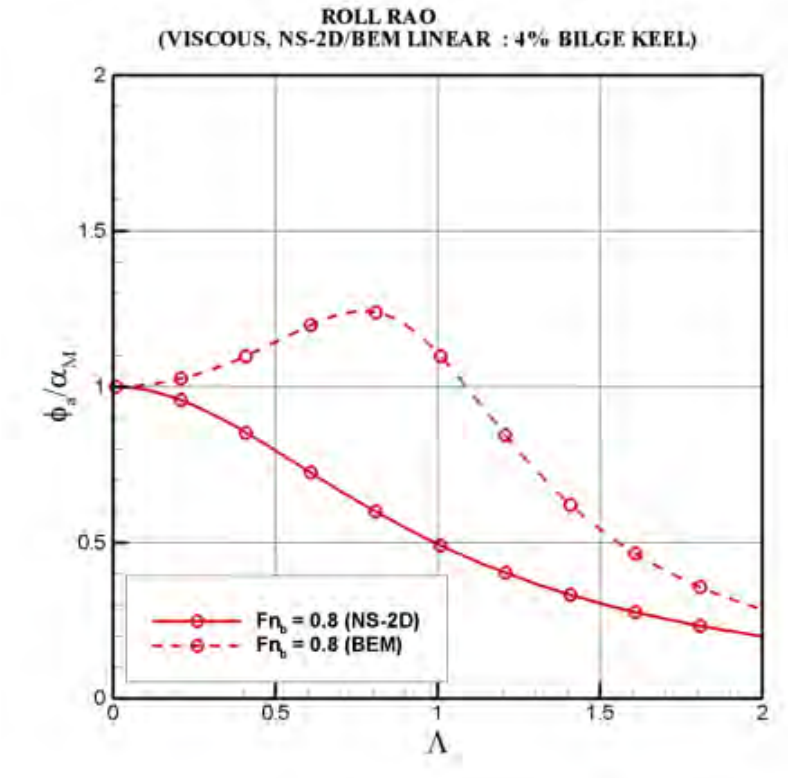

Figure D.9: Comparison of RAOs for Fn_b=0.8; Viscous and Inviscid results with 4% BILGE KEELS

Unit Conversion Chart

Conversion Factors for Different Units of Measurements			
Quantity	**SI Unit**	**Other Unit**	**Inverse Factor**
Length	1m	3.281 feet (ft)	0.3048 m
	1 km	0.540 nautical miles	1.852 km
	1 km	0.6213712 mile	1.609344 km
Area	1 m^2	10.764 ft^2	0.0929m^2
Volume	1 m^3	35.315 ft^3	0.0283 m^3
	1 m^3	264.2 gallon (US)	0.00379 m^3
	1 m^3	220.0 gallon (UK)	0.00455 m^3
	1 m^3	6.29 barrel (US Petroleum)	0.1589 m^3
Velocity	1 m/s	3.281 ft/s	0.305 m/s
	1 m/s	1.943 knot	0.515 m/s
	1 m/s	2.2369 mph	0.44704 m/s
	1 km/hr	0.62137 mph	1.6093 km/hr
Mass	1 kg	2.205 pound	0.454 kg
	1 Mg	0.984 ton (long)	1.016 Mg
	1 Mg	1 tonne (metric)	1 Mg
Force	1 N	0.225 pound force	4.448 N
	1 MN	100.4 ton force	9964 N
	1 MN	224.81 kip	4448 N
Pressure	1 N/m^2	0.000145 psi	6895 N/m^2
	1 MN/m^2	20.885 kip/ft^2	47880 N/m^2
Energy	1 J	0.738 foot pounds	1.356 J
Power	1 W	0.00134 horsepower	745.7 W
Temperature	0^0 Celsius	32^0 Fahrenheit	-17.78^0 Celsius
Frequency	1 cycle/s	1 hertz	1 cycle/second
Flow Rates	1 m^3/day	6.289 barrel/day	0.1589 m^3/day
	1 m^3/day	35.3146 ft^3/day	0.0283 m^3/day